Design of a FSAE Braking System

by

Luis Alberto Mora

Submitted to the
Department of Mechanical Engineering
in Partial Fulfillment of the Requirements for the Degree of

Bachelor of Science in Mechanical Engineering
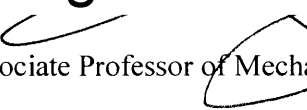
at the

Massachusetts Institute of Technology

June 2018
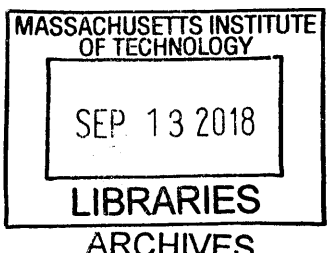
Signature of Author: _____ Signature redacted

Department of Mechanical Engineering
May 25, 2018

Certified by: _____ Signature redacted

Amos Winter
Associate Professor of Mechanical Engineering
Thesis Supervisor

Signature redacted

Accepted by: _____

Rohit Karnik
Associate Professor of Mechanical Engineering
Undergraduate Officer

1

MITLibraries

DISCLAIMER NOTICE

Due to the condition of the original material, there are unavoidable flaws in this reproduction. We have made every effort possible to provide you with the best copy available.

Thank you.

The images contained in this document are of the best quality available.

Design of a FSAE Braking System

by

Luis Alberto Mora

Submitted to the Department of Mechanical Engineering
on May 23, 2018 in Partial Fulfillment of the
Requirements for the Degree of

Bachelor of Science in Mechanical Engineering

ABSTRACT

MIT Motorsports is a FSAE Electric team at MIT that designs, manufactures, and tests electric formula style racecars to compete in an annual international collegiate design competition. The braking system for the MY18 vehicle developed by MIT Motorsports must enable the driver to consistently and reliably decelerate the vehicle at the maximum rate allowed by the traction limit of the tires. Crucial engineering data needed for a well-informed design, such as the coefficient of friction of the brake pads, motivated the development of a custom brake dynamometer to empirically test for the required data. The brake dynamometer became a very valuable tool eventually being used to select an appropriate brake rotor material and the most effective cooling geometry for the brake rotors. The braking system also integrates a regenerative braking system that works in parallel with the hydraulic braking system for the purpose of recovering braking energy and thus increasing vehicle efficiency. The MY18 braking system, will increase the maximum vehicle deceleration by 50% compared to MY17 and allow for up to 1kW-Hr more of energy recovery compared to MY17 without compromising reliability or consistency.

Thesis Supervisor: Amos Winter
Tile: Associate Professor of Mechanical Engineering

Table of Contents

1. INTRODUCTION

1.1 FORMULA SAE

Formula SAE is a collegiate design competition hosted by the Society of Automotive Engineers. The premise of the competition is to design, manufacture, and race a small formula style racecar that could be marketed to the causal track day autocross driver. Teams from many collegiate institutions from around the world compete in the various Formula SAE or Formula Student competitions hosted every year. In the United States there are 2 Formula SAE competitions and a Formula SAE Electric competition. At these competitions, student designs are judged for the design, cost, presentation, and the on-track performance of their vehicles. Some of the top performing FSAE cars have broken world records for straight line acceleration, and many industries heavily recruit students from Formula SAE teams.

1.2 MIT MOTORSPORTS

MIT Motorsports is the Formula SAE Electric team at the Massachusetts Institute of Technology in Cambridge, Massachusetts. The team designs small formula style, all-electric, battery powered racecars and has competed in the Formula SAE Electric competition in Lincoln, NE for the past 4 years. The team is comprised of a variety of engineering students at MIT, working together to create a reliable and high performing vehicle. The students manage the design, manufacturing, and testing processes for their car, and are responsible for all engineering decisions. The team achieved a second place overall finish at the 2017 competition with the MY17 vehicle. The MY17 vehicle is a rear wheel drive vehicle, with a custom battery pack, 18 in diameter Hoosier tires, with a vehicle weight of 507 lbs. The architecture of the vehicle was developed from first principles, abandoning the architectures of previous vehicle built by MIT Motorsports. MY17 was electrically and mechanically reliable, all while achieving top of class performance at the competition. MY18 is the vehicle currently in production for the FSAE Electric competition in June 2018. It is largely an evolution of the MY17 car, with key upgrades in the powertrain, braking, cooling, and electrical subsystems.

1.3 INTRODUCTION TO BRAKING SYSTEMS

In passenger road vehicles braking systems are a crucial safety system that allow drivers to reduce the speed of the vehicle to avoid collisions, maneuver traffic, and maintain safe travelling speeds. For racecars, the primary function of the braking system is to allow the driver to decelerate the vehicle at the maximum rate possible. The main difference between passenger and racing vehicle braking systems is that racing braking systems must endure much higher temperatures and stresses throughout an entire race. In FSAE spec racecars, the typical braking system consists of a direct acting hydraulic braking circuit acting on the brake calipers, with solid rotors attached to the hubs of the vehicle. The brake rotors are designed with cutouts such that the rotor and pad temperatures do not exceed the limits of the materials.

2. BACKGROUND

Issues in the MY17 braking system were identified prior to beginning the design process of the MY18 braking system, with the intention of addressing these issues with the new design. The main issue with the MY17 braking system was its failure to allow the driver to consistently bring the car to the maximum deceleration rate. The maximum deceleration rate of the MY17 vehicle was measured at approximately 0.9g's of deceleration. Given that the tire coefficient of friction is about 1.4, a 1.4g deceleration rate was expected to be the maximum.

Upon further investigation of this issue, three major problems were identified in the design of the MY17 braking system.
1. The mechanical advantage of the braking pedal was too low. In other words, an excessive amount of driver force would be required to bring the vehicle to maximum deceleration.
2. The coefficient of friction of the brake pads used in the calculations for the design of the MY17 braking system was over-estimated. In practice, this meant that the braking system was not producing the calculated braking torque per unit of driver input force that was expected.
3. During a testing session with the vehicle, the brake fluid boiled, causing the driver to lose the ability to bring the car to a stop. This failure indicates that the brake fluid temperature exceeded the boiling point of the DOT4 brake fluid being used.

These issues did not allow the driver to bring the vehicle to the maximum deceleration rate possible. The MY18 brake system designs addresses these issues as well as improves upon the design process for the braking system.

The system level goals for the MY18 braking system is as follows:
- The braking system will enable the driver to consistently and reliably decelerate the vehicle at the maximum rate allowed by the limit of traction of the tires, for an entire 22km long endurance race, if not longer.
- The braking system hardware must be designed such that regenerative braking software can be integrated into the braking system.

2.1 FIRST PRINCIPLES

With the system level goal defined, the physics of a braking event was studied using first principles. The car is first modeled using the bicycle model; it consists of a center of mass, and two axles and wheels (front and rear). Gravity and other accelerations act on the center of mass, normal forces and friction forces act on the tire contact points with the ground, and aerodynamic forces act on the center of gravity. During a braking event, a negative acceleration (deceleration) will be applied at the center of mass. The normal forces acting on the front and rear tires will be a function of the vehicle acceleration. Aerodynamic downforce can be added to the normal forces calculated from the change in normal force due to acceleration. The force of friction available at the front and rear tires can be calculated by assuming an average constant coefficient of friction for the tires. Then drag forces can be added to the friction forces, and Newton's first law can be used to determine the resulting acceleration. At this point the new calculated acceleration can be

used once more to calculate new normal forces; this iteration process will eventually converge to a maximum possible deceleration rate.

Once the friction force available at the front and rear axles is defined at a particular deceleration, Newton's first law can be applied for the wheel itself. The wheel body will have the force of friction acting at the tire contact point with the ground, a braking torque acting on the wheel, the wheel itself will have an angular acceleration and a rotational moment of inertia. The product of the angular deceleration and the moment of inertia of this system happens to be a value close to zero, therefore it is neglected. Newton's first law then becomes a torque balance equation, and the braking torque required to meet the friction force available at the tire can be calculated.

To augment these simple calculations, a commercial lap time simulator (LTS) software package called OptimumLap was used to calculate the braking force as a function of position and time on the simulated race course. Vehicle parameters that mathematically described the MY18 vehicle, and a track representative of the FSAE endurance course were used as inputs to the LTS study to generate a wide variety of outputs. Using the velocity and force output of the simulation, braking power as a function of time was calculated.

The torque requirement for the braking system on the front and rear axles is now defined, which can be used to design the hydraulic circuit used to actuate the brakes. The power requirement for the braking system is also defined by the braking power output of the LTS study, which can be used to define the steady state cooling requirements for the braking system to ensure consistent, reliable performance.

2.2 BRAKING SYSTEM ARCHITECTURE

The braking system architecture is largely independent from the torque and power requirements defined by first principles. The architecture was based on MY17's braking system with some key changes to better accommodate the regenerative braking goals.

Starting at the wheels, braking torque is provided at all four wheels with a solid floating disc rotor and fixed brake calipers with semi metallic brake pads. The brake calipers are actuated with two independent hydraulic braking circuits for the front and rear axles. Each hydraulic circuit consists of a reservoir, a master cylinder, a series of lines and fittings, and two calipers in parallel. The master cylinders are attached to the brake pedal with a bias bar, a mechanism that can be used to adjust the distribution of braking force, front to rear. The brake pedal geometry gives the driver mechanical advantage to amplify the force input of the driver to a larger force input on the master cylinders.

To allow for the integration of a regenerative braking system, the braking system has pressure transducers for each of the hydraulic circuits. In addition, a brake shutoff solenoid valve is used in the rear hydraulic braking circuit to "cut" pressure to the rear hydraulic brakes, to maximize the amount of work done by the electric motor and maximize the energy recovery.

6

3. DESIGN

The design process for the brake system is as follows:
- The first step in the design is to gather the required data for the hydraulic system design. From the equations governing the hydraulic system pressures and forces, the need for accurate driver force data, and brake pad coefficient of friction data becomes obvious.
- The hydraulic system can now be designed. It involves evaluating the specifications of off the shelf components and selecting appropriate parts for the system. In addition, the hardware necessary for regenerative braking is integrated into the hydraulic system.
- The brake rotor assembly is then designed. The design of the brake rotors is greatly augmented by empirical data collected on a custom brake dynamometer. For example, the brake rotor material is selected using the coefficient of friction vs temperature relationship to determine the best material for the application.
- Finally, a regenerative braking control scheme is developed and shared with the vehicle's software team for implementation.

3.1 BRAKING SYSTEM EQUATIONS

The braking torque requirement for the front and rear axles can be calculated from the following equation given that the normal force, F_z, at each of the axles and the tire radius, r_{tire}, is known during a braking event.

$$\tau_{braking,f} = r_{tire} \cdot F_{z,f} \cdot \mu_{tire} \tag{1}$$

$$\tau_{braking,r} = r_{tire} \cdot F_{z,r} \cdot \mu_{tire} \tag{2}$$

Note that these equations assume a constant coefficient of friction, μ_{tire}, for the tires. In reality the coefficient of friction is sensitive to normal force acting on the tire, but for the purposes of designing the hydraulic braking system, it is acceptable to use an average coefficient of friction for the tires.

The hydraulic braking system is a hydrostatic pressure system, with an incompressible fluid, meaning that the calculation of forces and pressures is very simple. Recall that the brake pedal is attached to two independent master cylinders with a bias bar that distributes force from the pedal to each master cylinder. The master cylinder output pressure is proportional to the force input to the master cylinder. There is no pressure drop in any of the brake lines between the master cylinders and the brake calipers, since there is no fluid flow or any kind of pressure regulator device. Pressure from the brake lines applies force on the pistons in the brake calipers, applying a clamping force on the brake pads and rotors. The friction force of the brake pads acts at an effective brake rotor radius and results in braking torque. The following equations map driver input force at the pedal, to a resulting braking torque.

$$F_{driver} \cdot PR \cdot BB_f = \frac{\tau_{braking,f} \cdot A_{MC,f}}{2 \cdot r_{rotor,effective} \cdot \mu_{pad-rotor} \cdot A_{C,f}} \tag{3}$$

$$F_{driver} \cdot PR \cdot BB_r = \frac{\tau_{braking,r} \cdot A_{MC,r}}{2 \cdot r_{rotor,effective} \cdot \mu_{pad-rotor} \cdot A_{C,r}} \tag{4}$$

Note that PR is the pedal ratio, which is defined as the ratio of force being applied on both master cylinders, divided by the driver input force. BB_f represents the fraction of the driver force being applied to the front master cylinder. BB_r is similar but for the rear master cylinder. On the right hand side of the equation, the master cylinder area, A_{MC}, and caliper piston area, A_C are relevant.

Also note that to achieve the desired braking torque at the desired driver force, the rotor effective radius, $r_{rotor,effective}$, master cylinder and caliper piston areas, and the pedal ratio can all be adjusted to meet the requirement.

The following equation relates the hydraulic pressure in the system to the driver input force.

$$P_{hydraulic,f} = \frac{F_{driver} \cdot PR \cdot BB_f}{A_{MC,f}} \tag{5}$$

$$P_{hydraulic,r} = \frac{F_{driver} \cdot PR \cdot BB_r}{A_{MC,r}} \tag{6}$$

Hydraulic pressure, $P_{hydraulic}$ is important because the components in the circuit have a maximum rated hydraulic pressure that must not be exceeded. This equation thus helps constrain the selection of an appropriate pedal ratio and master cylinder area.

The final equation that needs to be considered for this system describes the bias bar.

$$BB_f + BB_r = 1 \tag{7}$$

3.2 BRAKE DYNAMOMETER

From equations (3) and (4) it is notable that the coefficient of friction of the brake pad plays a big role in the mapping of driver input force to braking torque at the wheels. Unfortunately, for the brake pads being considered for this system, the manufacturer was not willing to provide data for average coefficient of friction values. Also recall that an overestimate of this average friction coefficient was a major issue in the MY17 design. The ultimate effect was that the driver would have to apply an excessive amount of force to get the vehicle to decelerate at the traction limit of the tires.

The coefficient of friction of the brake pads is also a function of temperature, as well as a function of the rotor material, not just the pad material. Even if the manufacturer had released data for an average coefficient of friction, it would have only been for a particular rotor material, most likely cast iron. Having the coefficient as a function of temperature was also important since one of the main goals of the system is to provide consistent braking throughout an entire race. If the coefficient is really sensitive to temperature, then the braking effort the driver will need to exert will change as the brake pads heat up and cool down.

This need for detailed friction coefficient data motivated the development of a custom brake dynamometer for the purposes of collecting this data. Having a brake dynamometer would also be useful in the thermo-mechanical design of the brake rotors, allowing us to empirically measure the thermal resistance of a particular rotor cooling geometry.

The brake dynamometer that was built is pictured in figure 1. It is driven by a 3 phase electric motor, controlled by a digital inverter, with the brakes providing a load to the motor. A chain and sprocket gear reduction brings the speed of the motor down to the right range for the brakes. The brake dynamometer is contained in a simple steel box frame, with a series of aluminum bearing supports for the various shafts.
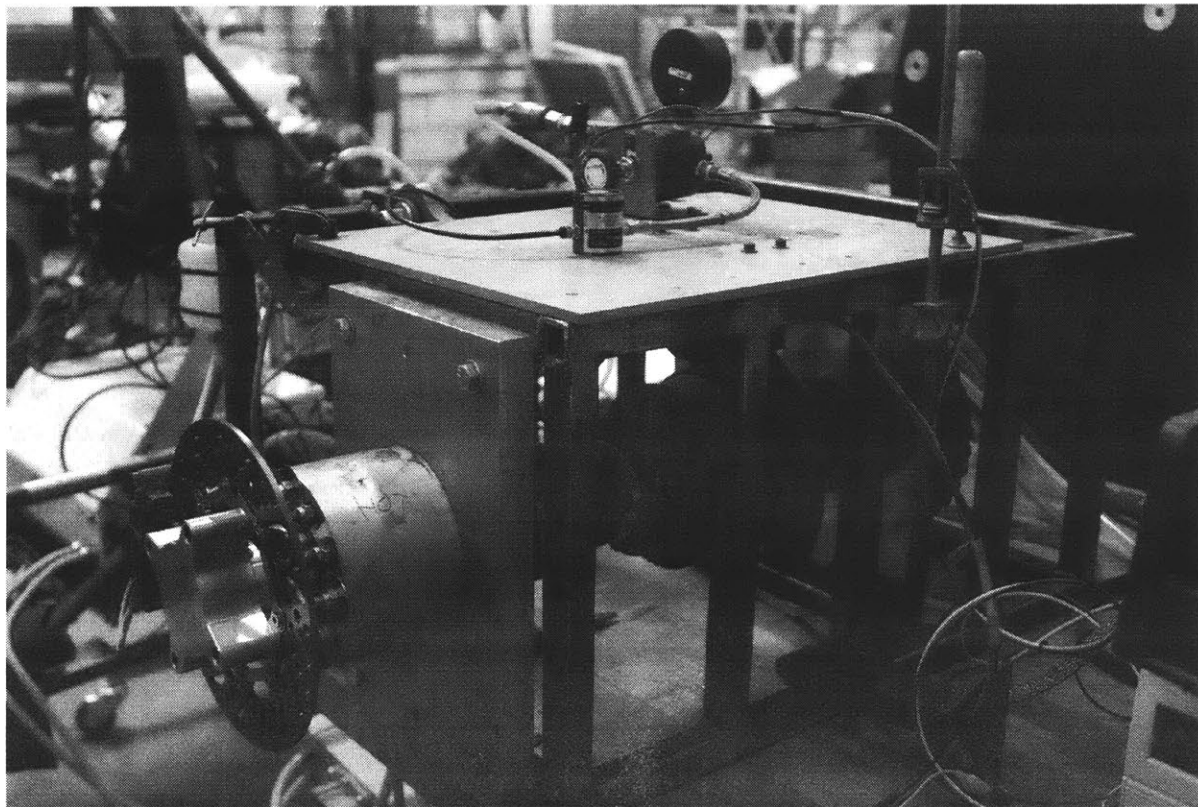

Figure 1. Custom self-developed brake dynamometer. Consists of a pneumatic-hydraulic remote brake actuation system, a rotary torque sensor, and it is powered by MY18's electric powertrain. Sensors include, a 500 Nm rotary torque sensor, embedded brake pad thermocouples, hydraulic pressure transducer, and a FLIR thermal imaging camera.

To be able to measure the coefficient of friction, three variables need to be measured: hydraulic pressure acting on the brake calipers ($P_{hydraulic}$), the torque produced by the brakes as measured on the wheel hub ($\tau_{braking}$), and the temperature of the brake pad (T_{pad}).

Combining equations (4) and (6) results in equation (8), which can be used to calculate $\mu_{pad-rotor}$, as a function of T_{pad}. Note that the rotor effective radius and the caliper piston area are known quantities.

$$\mu_{pad-rotor} = \frac{\tau_{braking,r}}{2 \cdot r_{rotor,effective} \cdot P_{hydraulic,f} \cdot A_{C,r}} \tag{8}$$

There are four sensors used with the brake dynamometer. First is a rotary torque sensor: Interface HRDT 500 Nm. It allows for an accurate measurement of braking torque. The second is a pressure transducer used to measure hydraulic braking pressure: a TE MEAS MSP300 pressure transducer. The third is an embedded brake bad k type thermocouple used to measure the bulk brake pad temperature: a HGSI BPTC thermocouple. Finally, a FLIR thermal imaging camera was used to measure rotor surface temperatures.

The brake dynamometer is powered by the electric powertrain used in the MY18 vehicle. The electric motor is the Emrax 228, controlled by the RMS PM100DXR inverter, drawing power from the MY18 300V battery pack.

The braking system on the dynamometer is actuated by a pneumatic hydraulic system. A pneumatic cylinder applies force on the hydraulic master cylinder through a lever arm. Air pressure into the pneumatic cylinder is controlled with an upstream solenoid valve and a 0 to 100 PSI pressure regulator. The regulator and the solenoid valve allow for the remote control and actuation of the brake caliper, with braking force being provided by a high pressure source as opposed to the user.
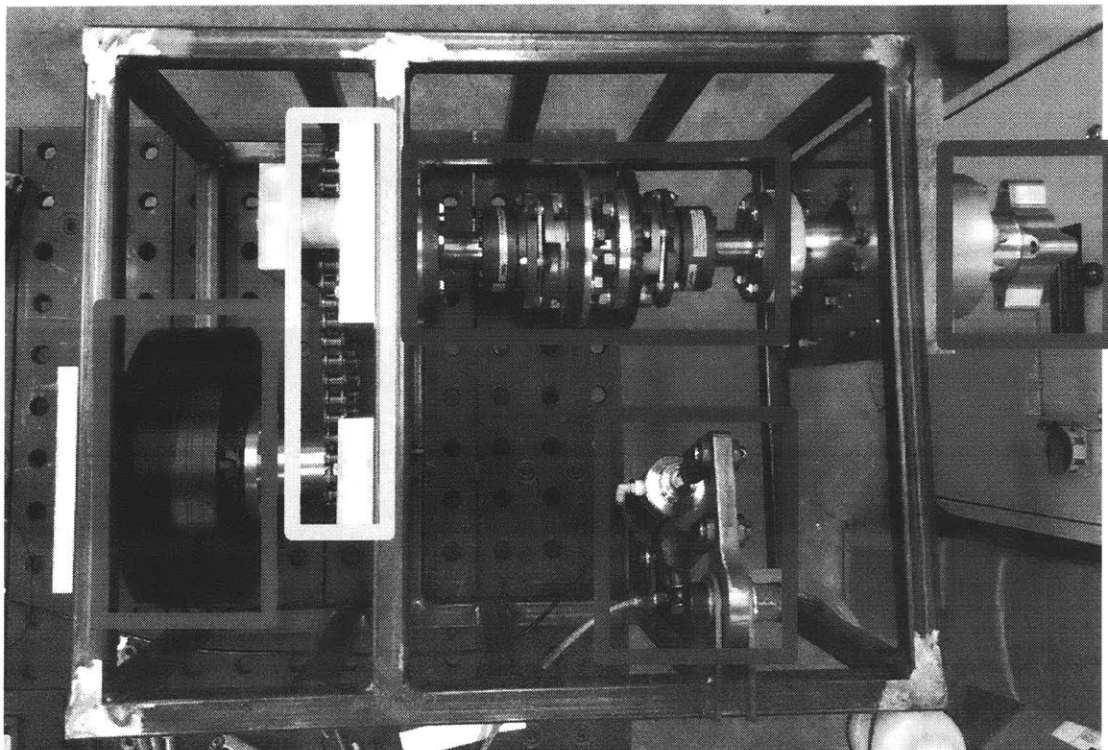
Figure 2. Brake dynamometer components. Green box: electric motor. Yellow box: sprocket and chain gear reduction. Red Box: rotary torque transducer. Purple box: remote pneumatic-hydraulic brake actuation. Blue box: simulated hub and wheel upright assembly.

3.3 HYDRAULIC SYSTEM

The hydraulic system is defined as the part of the braking system that is hydraulically actuated and applies a clamping force at the brake calipers. This includes everything in the hydraulic circuit, from master cylinders to the brake calipers.

3.3.1 BRAKE CALIPERS

The brake calipers for the system were selected first. The MY17 braking system used the Wilwood GP200 brake calipers on all four wheels. With a weight of less than 1lb and a cost of less than $100 each they were a very lightweight economical choice. Other similar calipers were either more expensive, larger, heavier, or not readily available to merit changing calipers. The MY18 braking system, therefore uses 4 GP200 calipers at all four wheels. Wilwood claims that the maximum pressure must not exceed 1200 PSI. After speaking directly with the manufacturer, it was discovered that this pressure rating was developed by causing a cycle fatigue failure with cycles of 1200 PSI. This is not indicative of the ultimate maximum pressure rating. Wilwood would not release engineering data regarding the ultimate maximum pressure rating of their caliper.

Defining the maximum and operating pressures for the hydraulic system is an important way to ensure the safety and reliability of the system. Each of the components in the hydraulic circuit must be capable of surviving a maximum pressure event, which may occur if the driver exerts a

11

large amount of force on the brake pedal in an emergency situation. The operating pressure should be defined as the normal expected pressure the driver exerts when in racing conditions. All components should be able to handle a large number of loading cycles at the operating pressure, which may be significantly below the ultimate maximum pressure rating.

In order to determine the ultimate maximum pressure rating of the GP200 brake calipers, a destructive test was instrumented to find the failure pressure point of the calipers. A GP200 brake caliper was attached to a master cylinder and a pressure transducer. The pressure on the brake caliper was gradually increased until the brake caliper mechanically failed. Figure 3 shows the results of this test. The brake caliper burst at approximately 5000 PSI of pressure. Note that while it was suspected that the calipers were going to fail first the test also served to test the capability of the master cylinder, brake lines, and the pressure transducer.
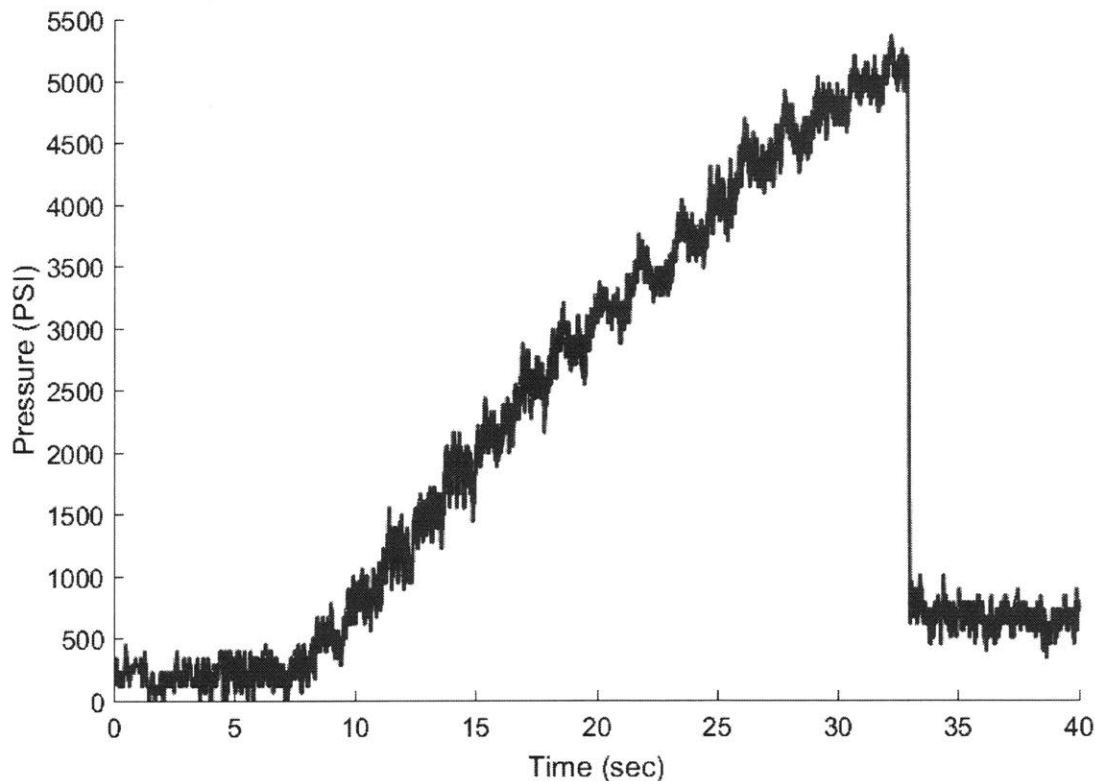

Figure 3. Wilwood GP200 caliper burst pressure test. The brake caliper was destructively tested to determine the maximum burst pressure. The caliper failed at 5000 PSI of hydraulic pressure.

In summary the following pressure ratings were determined for a hydraulic system using GP200 brake calipers:

      Maximum operating pressure = 1200 PSI
      Ultimate maximum pressure = 5000 PSI

A minimum coefficient of friction requirement can be calculated with equation (8) based on the maximum operating pressure of the brake calipers, the brake caliper piston area, and the maximum torque requirement. This requirement can be used later in the brake rotor material selection process to ensure that whatever material is chosen can still bring the car to maximum deceleration.

Minimum brake pad coefficient of friction = 0.32

3.3.2 BRAKE ROTOR RADIUS

The brake rotor radius can be selected. From equation (3) it is evident that maximizing the rotor radius lowers the required driver effort. The brake caliper and the brake rotor must fit within the wheel rim, which has a useable inner diameter of about 9.5 in. Given the sizing of the Wilwood GP200 caliper the maximum rotor diameter was determined to be 8 in. The effective rotor radius was therefore 3.375 in.

3.3.3 MASTER CYLINDERS

The master cylinder areas can now be selected as well. For this system the Tilton 78 Series master cylinders were selected. They offer a range of master cylinder bore diameters from 5/8" to 1". They are also readily available and less expensive than comparable master cylinders made by AP Racing. The 78 series cylinders are also configured as 2 force members, with a spherical bearing on one end and a clevis on the other end, making them ideal for integration into the pedal box. From equation x and y, one can solve for the ratio of braking torque in the front divided by the rear. This ratio is proportional to the ratio of the front and rear master cylinder areas given that the caliper piston areas and the rotor effective radii are the same on all four wheels. Given a front braking torque requirement of 384 Nm and a rear braking torque requirement of 145 Nm per wheel, the appropriate master cylinder bore sizes could be selected:

Front master cylinder bore diameter = 5/8"
Rear master cylinder bore diameter = 1"

3.3.4 PEDAL RATIO

The final parameter that needs to be specified is the pedal ratio for the pedal box. Recall that the pedal ratio is defined as the ratio of the amount of force acting on both master cylinders, divided by the force input from the driver. It provides the driver with some mechanical advantage over the master cylinders to be able to apply enough hydraulic pressure.

Also recall that the MY17 vehicle had a pedal ratio value that was too low; it was specified as 2.7. The pedal ratio on MY17 was measured and it was discovered that the as-built pedal ratio was 2.4, and thus made it even more difficult to bring the brakes to the limit of traction. The calculation for the pedal ratio depends on the brake pad coefficient of friction value and the desired nominal driver input force.

An experiment to determine the optimal driver input force was conducted for the purposes of selecting the correct pedal ratio. A number of drivers we asked to sit in the cockpit of MY17 and press on the brake pedal with a force they believed they could sustain lap after lap in an endurance

race and bring the car to the traction limit. Although preference among drivers differed, a range of forces from 900N to 1050N seemed reasonable given the empirical data from the experiment.

At the point in time when the pedal ratio needed to be decided, the coefficient of friction of the pad-rotor interface was still untested. To allow for the development and fabrication of the pedal box to proceed on schedule the minimum brake pad coefficient of friction of 0.32 was sued in the calculation of the PR. Furthermore, it was requested that the pedal ratio be adjustable by +/- 10% so that the final value could be fine-tuned at a later date. A pedal ratio of 3.14 was specified and passed along as a requirement to the pedal box team that was responsible for designing the pedal geometry.

3.3.5 BRAKE LINES, VALVES, AND FITTINGS

The hydraulic brake lines distribute the hydraulic brake pressure generated from the master cylinders to the pressure transducers and the brake calipers. The brake lines are terminated with 3AN 37 degree flared fittings, and are a variety of flexible hose line and stainless steel lines. Stainless steel bulkhead t-fittings are used to secure the lines to the chassis. Flex lines near the pedal allow for the pedal box to be adjusted to various positions for different drivers without needing to bend or otherwise modify the brake lines.

The front and rear brake lines each have a pressure transducer attached at a t-fitting to measure the hydraulic pressure in the front and rear hydraulic braking circuits. The transducers use an 1/8" NPT t-fitting. The transducers were selected to produce a 0.5-4.5 V output, with a measureable range up to 1500 PSI, slightly above the 1200 PSI nominal operating pressure of the hydraulic system. The maximum overload pressure for the transducer is three times the measurable range, putting the maximum allowable pressure at 4500 PSI. The transducers selected for the system are GEMS 3200 series thin film pressure transducer.

The rear brake lines also feature a Wilwood Brake Shut Off Solenoid Valve. The valve is placed upstream from the pressure transducer. The function of the shut-off valve is to provide the vehicle's VCU a means to "shut off" the rear hydraulic brakes. When the solenoid valve is powered with 12V, it closes its valve, meaning that high pressure at the inlet port of solenoid valve does not continue to the outlet port of the solenoid valve. With the solenoid valve in the closed position, pressing the brake pedal only applies braking torque in the front axle. This is desirable for the purposes of regenerative braking. Since the vehicle has a rear wheel drive electric powertrain, the electric motor can apply a braking torque at the rear wheels, and recover that braking energy. To maximize the amount of energy recovered, the rear hydraulic brakes are completely disabled so that the electric motor is providing 100% of the braking torque required.

Recall that one of the main issues with the MY17 braking system was that the brake fluid exceeded the boiling point and caused the brakes to fail during a testing session. MY17 initially used DOT4 braking fluid, which has a dry boiling point of 230°C. The MY18 braking system uses Castrol SRF Race Braking Fluid which has a dry boiling point of 300°C. This new braking fluid was tested on the MY17 vehicle in the fall of 2017, and the new braking fluid improved the reliability of the braking system.

3.4 BRAKE ROTOR DEVELOPMENT

Brake rotor development for the MY18 vehicle was an extensive process. A majority of the design time for the entire braking system was devoted to the design of the brake rotor assembly. This is largely due to the fact that the brake dynamometer made it possible to study many details about the brake rotor performance. Furthermore, the brake rotor itself could have a large impact on the reliability and the consistency of the braking system. The main improvements in the design of the brake rotors include, increased build quality with a massive improvement in rotor flatness and runout, improved floating rotor mechanism, consistent coefficient of friction across the entire temperature range and better cooling performance.

3.4.1 ROTOR MATERIAL SELECTION

A number of materials were considered suitable candidates for use in the brake rotors. A variety of alloy steels, stainless steels, and cast iron materials were considered. One of the main factors influencing whether or not a material would be considered for use in the rotors was the availability of trustworthy material property data. MMPDS-11 was used as a trustworthy material property database. MMPDS-11 is widely used in the aerospace industry for the same purpose. Materials are indexed by their AMS specifications and properties such as strength, modulus, heat capacity, and S-N curves are provided for a wide variety of alloys, in different forms, or heat treatments. Figure 4 shows an example of a strength vs temperature plot available in MMPDS-11.
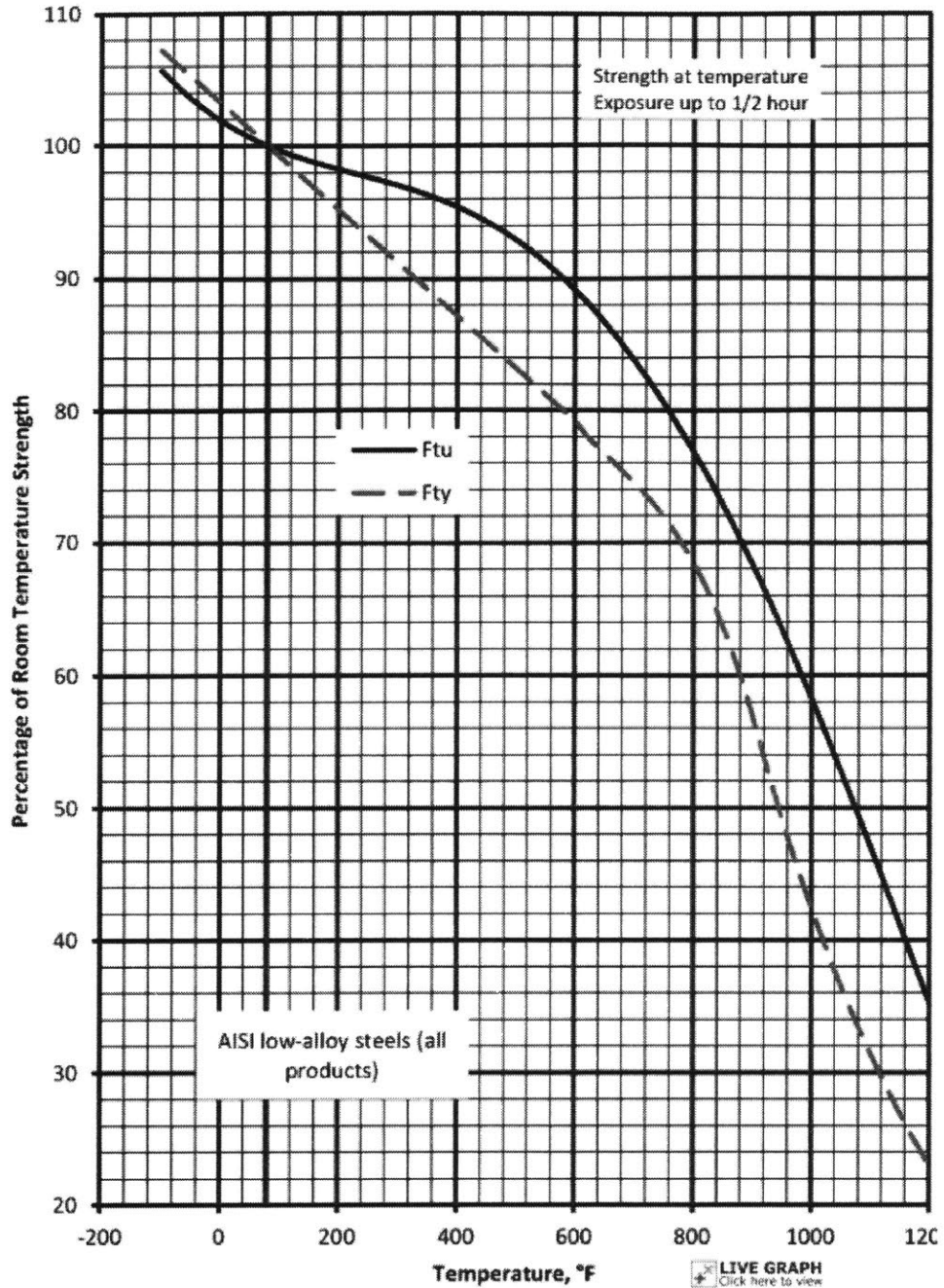
Figure 2.3.1.1.1. Effect of temperature on the tensile ultimate strength (F_{tu}) and tensile yield strength (F_{ty}) of AISI low-alloy steels (all products).

Figure 4. Material strength vs temperature plot from MMPDS-11. This materials data resource was used as the source for engineering materials data including strength and its dependence on temperature, specific heat capacity, and elastic modulus. MMPDS-11 also provides AMS specifications for materials making it easier to procure high quality engineering materials for the braking system.

To be able to select a particular material for use in the brake rotors, three candidate materials would be tested on the brake dynamometer and the pad-rotor friction coefficient vs temperature curve for

each material and brake pad combination would be compared. The ideal material would have a coefficient of friction that was very consistent and constant throughout the entire temperature range of the brake pads. The material should also meet or exceed the minimum average friction coefficient calculated from the hydraulic system design.

While there were three brake rotor material candidates, there was only one brake pad compound available for testing. It is Wilwood's Composite Metallic Compound, which according to the manufacturer is designed for use at high temperatures. Numerical data for these brake pads is not provided.

The three candidate rotor materials are cast iron, 17-4PH stainless steel, and 4130 normalized steel alloy. Cast iron was considered because it is the most common brake rotor material in the world and most brake pads are optimized for use with cast iron. Cast iron has good thermal conductivity but very poor strength. Furthermore, cast iron lacks ductility meaning that it is prone to the formation of cracks under high stress. 17-4PH stainless steel has a very high strength but has about 40% of the thermal conductivity of cast iron. Finally, 4130 steel alloy was selected since it was the material chosen for the MY17 braking system. It has good strength and comparable thermal conductivity to cast iron.

Material properties for 17-4 and 4130 alloy were found in MMPDS-11. Cast Iron material properties were sourced from the manufacturer of G2 Durabar Cast Iron. However, MMPDS-11 contains more detailed information, specifically the yield strength as a function of temperature, which would eventually become an important factor in the design of the rotors.

A test procedure for the brake dynamometer was developed to be able to collect comparable friction coefficient data across the three different rotor materials. The procedure was meticulously reproduced on all tested rotors to maintain the fidelity of the results for later comparison. The procedure is as follows:
1. A brand new brake rotor and a set of brake pads is installed onto the brake dynamometer.
2. Both the rotor and the new brake pads must undergo a bedding procedure, which finalizes the curing process for the brake pads. The process is detailed on Wilwood's website.
3. Now the brake rotor and brake pads are ready for the test to begin. The DAQ loggers are started and the pneumatic pressure is set to 100 PSI. The motor RPM is set to 1250 RPM. The solenoid valve actuating the brake is pulsed, causing an impulse on the torque, pressure, and temperature. This is used later to synchronize the data logs.
4. The pneumatic pressure regulator is now set to 40 PSI. The motor RPM is still set to 1250 RPM. The operator then waits until the brake pad temperature reduces down below 100°C, at which point the operator then actuates the brake by opening the solenoid valve. The caliper is now applying a braking torque.
5. The temperature rises up to 500°C, at which point the operator closes the solenoid valve. This releases the brake caliper, and thus the braking torque drops down to zero.
6. At this point the rotor must be allowed to cool from 500°C down to 100°C. The motor RPM may be increased to increase the cooling rate.
7. The operator returns to step four, and repeats this process for at least 5 runs.

Figure 5 shows an example of what the raw data collected from the described test procedure looks like. Note that the raw data exhibits a lot of noise that is not ideal for making subsequent calculations. The raw data is filtered with a moving average, and is shown in the figure.
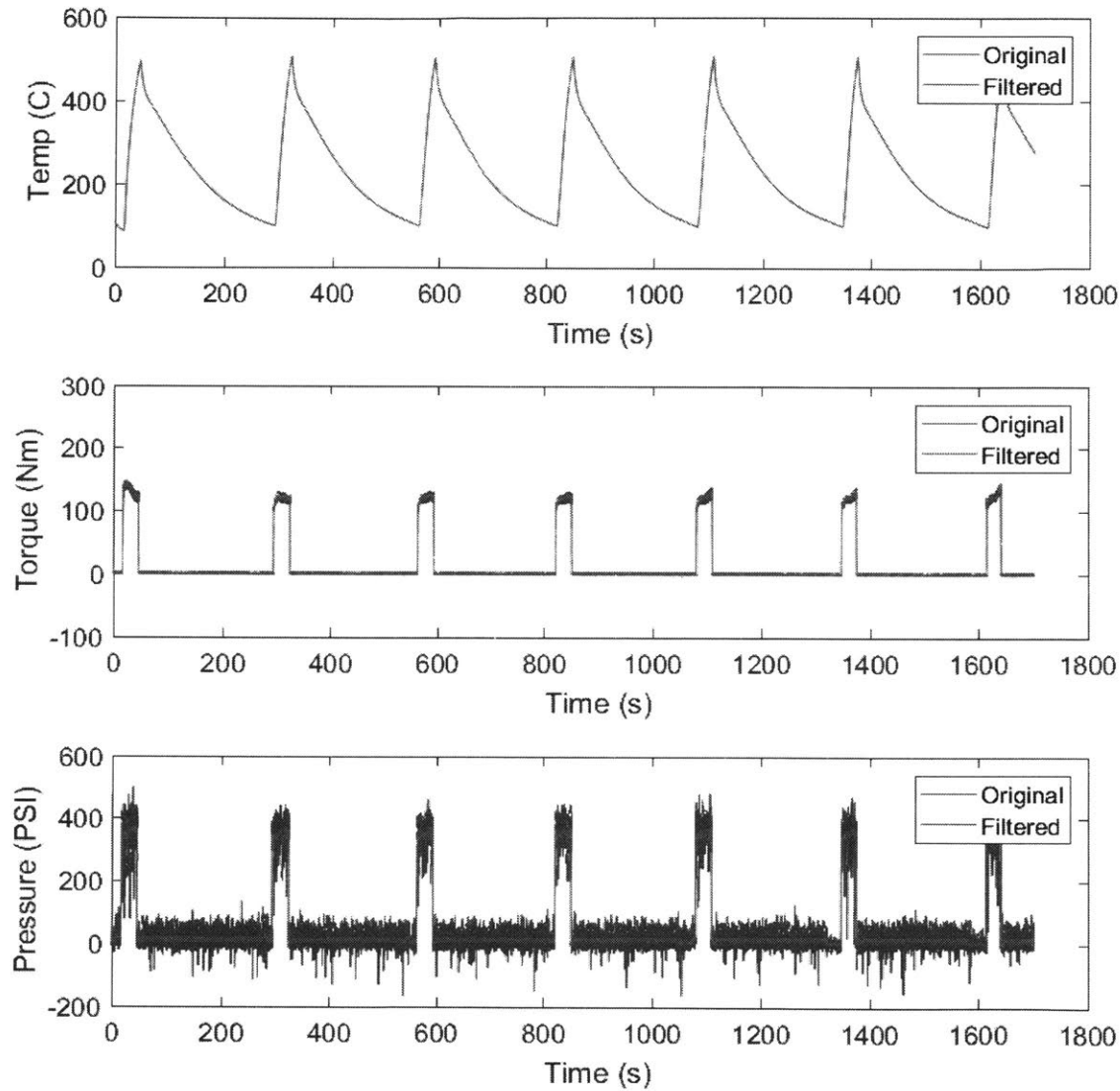

Figure 5. Typical pad-rotor mu vs temperature test profile. This data was collected using a custom self-developed brake dynamometer. The brake pad temperature, torque exerted by the brake rotor, and hydraulic pressure in the brake calipers is shown. The raw data exhibits noise due to EMI from the electric powertrain powering the brake dynamometer. The data was filtered to make it suitable for subsequent calculations.

The results from this test procedure can be used with equation (8) to produce the friction coefficient vs temperature plot. Figures 6. through 8. are the friction coefficient plots for cast iron, 17-4PH stainless steel, and 4130 steel alloy.
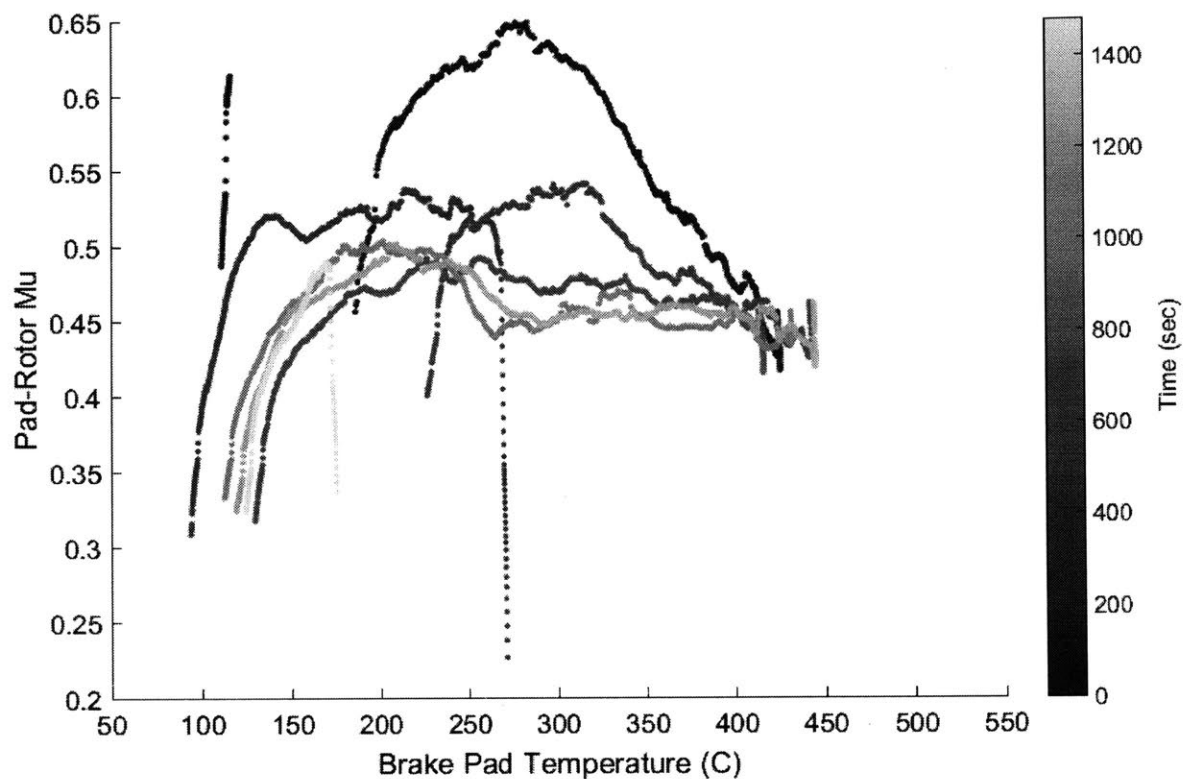

Figure 6. Mu vs temperature for cast iron rotors and CM compound brake pads. Shown in the colorbar is time, showing how the data changes from run to run. Note how the first run is an outlier in the data, indicating that there is a "run in" period before the brakes become more consistent.
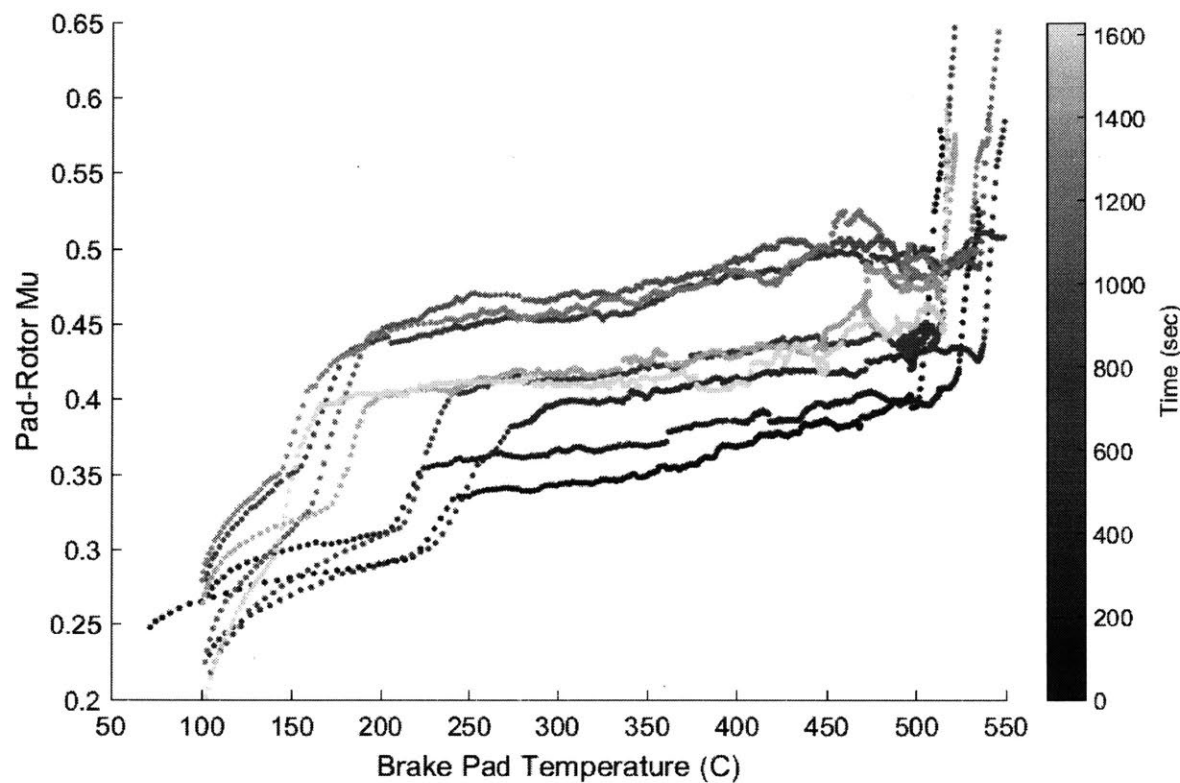
Figure 7. Mu vs temperature for 17-4PH stainless steel and CM compound brake pads. Shown in the colorbar is time, showing how the data changes from run to run. Note how the various runs are not consistent with each other, indicating that the coefficient of friction for this material is sensitive to pad wear or other untested variables.
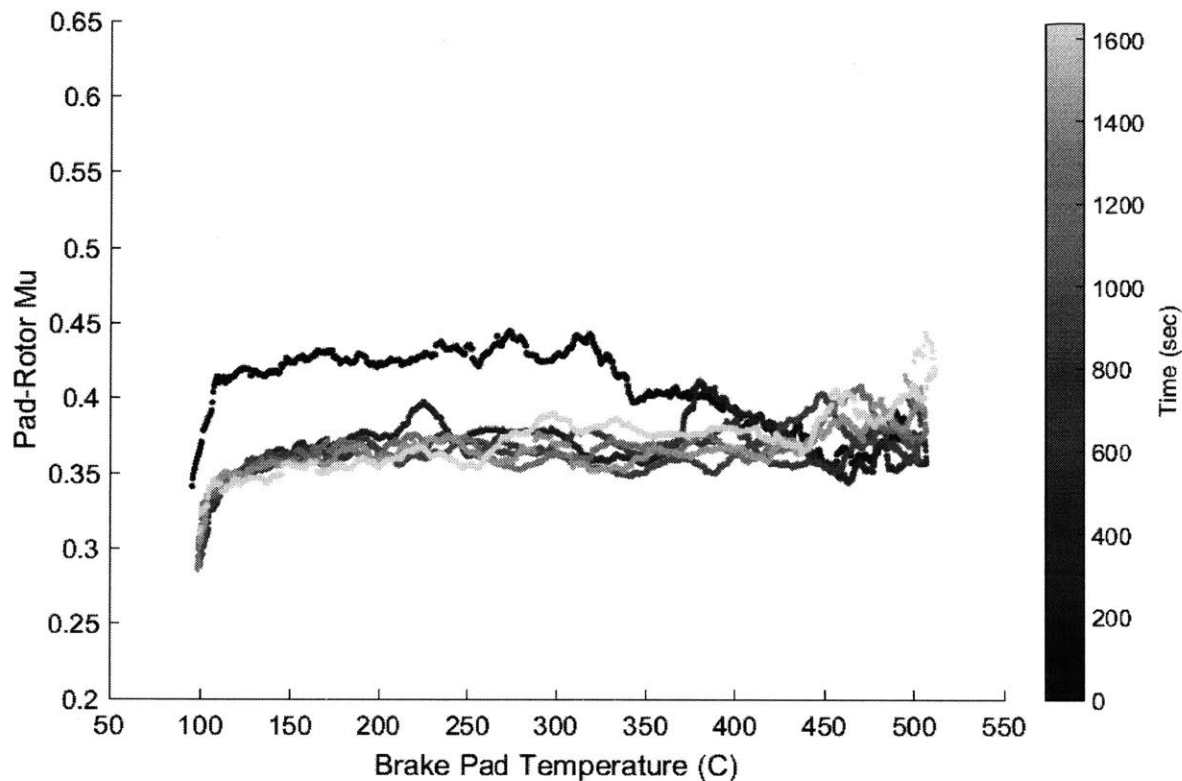
Figure 8. Mu vs temperature for 4130 alloy steel rotors and CM compound brake pads. Shown in the colorbar is time, showing how the data changes from run to run. Note how the first run is an outlier in the data, indicating that there is a "run in" period before the brakes become more consistent. Subsequent runs are very consistent with each other, indicating that this material and brake pad combination is very resilient to brake pad wear.

Note that a colorbar is used in these plots to visually differentiate the data from different runs in one experiment. This is important because it shows the dependence of the friction coefficient on the number of runs. The number of runs can be analogous to number of braking cycles; it can be concluded that a plot with overlapping curves will have a consistent friction coefficient with increasing braking cycles.

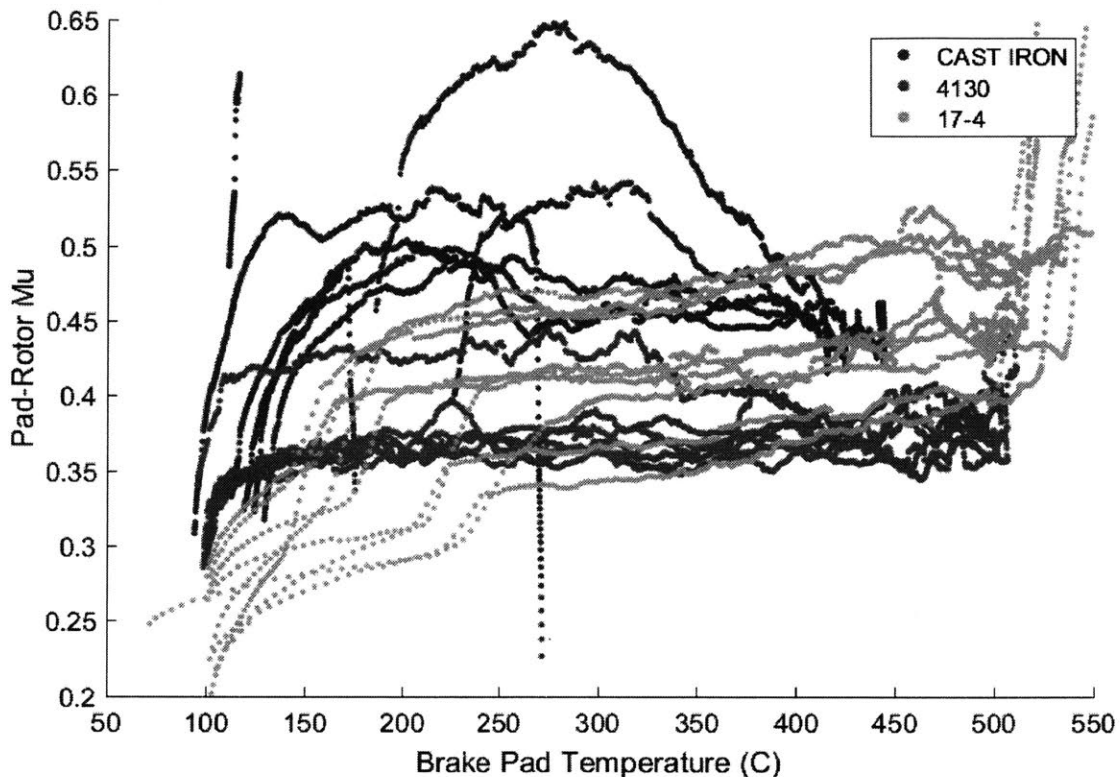Figure 9 shows a comparison of all three material's friction coefficient curves on one plot for ease of comparison.

Figure 9. Comparison of mu vs temperature for the tested rotor materials. Although 4130 steel alloy has the lowest average mu, its consistency across runs, and weak dependence on temperature made it the ideal material for the brake rotors. These properties are crucial in delivering a braking system that reliably and consistently allows the driver to decelerate the vehicle at the limit of traction.

A few conclusions can be made from this plot:
- Cast Iron exhibits the highest average friction coefficient, and 4130 has the lowest.
- 4130 alloy has a very flat friction coefficient curve, meaning that changes in temperature will not affect the amount of braking effort the driver needs to exert.
- 4130 alloy also has curves that overlap each other, indicating a very weak dependence on the number of braking cycles.
- On the contrary 17-4 stainless steel seems to have an inconsistent friction coefficient across a number of runs. It also exhibits a mild temperature dependence.

Upon visual inspection after these tests, it was discovered that the cast iron rotors had cracks propagating for the bolted joint from the rotor to the hub. Figure 10 shows these cracks. This mechanical failure was a result of cast iron's low strength and lack of ductility. The lack of ductility is particularly undesirable since it becomes easier for cracks to form, and for fracture to occur. Even though cast iron exhibited the highest average friction coefficient, it was neither the most consistent nor the most reliable. cast iron would not be a suitable material for the MY18 braking system.
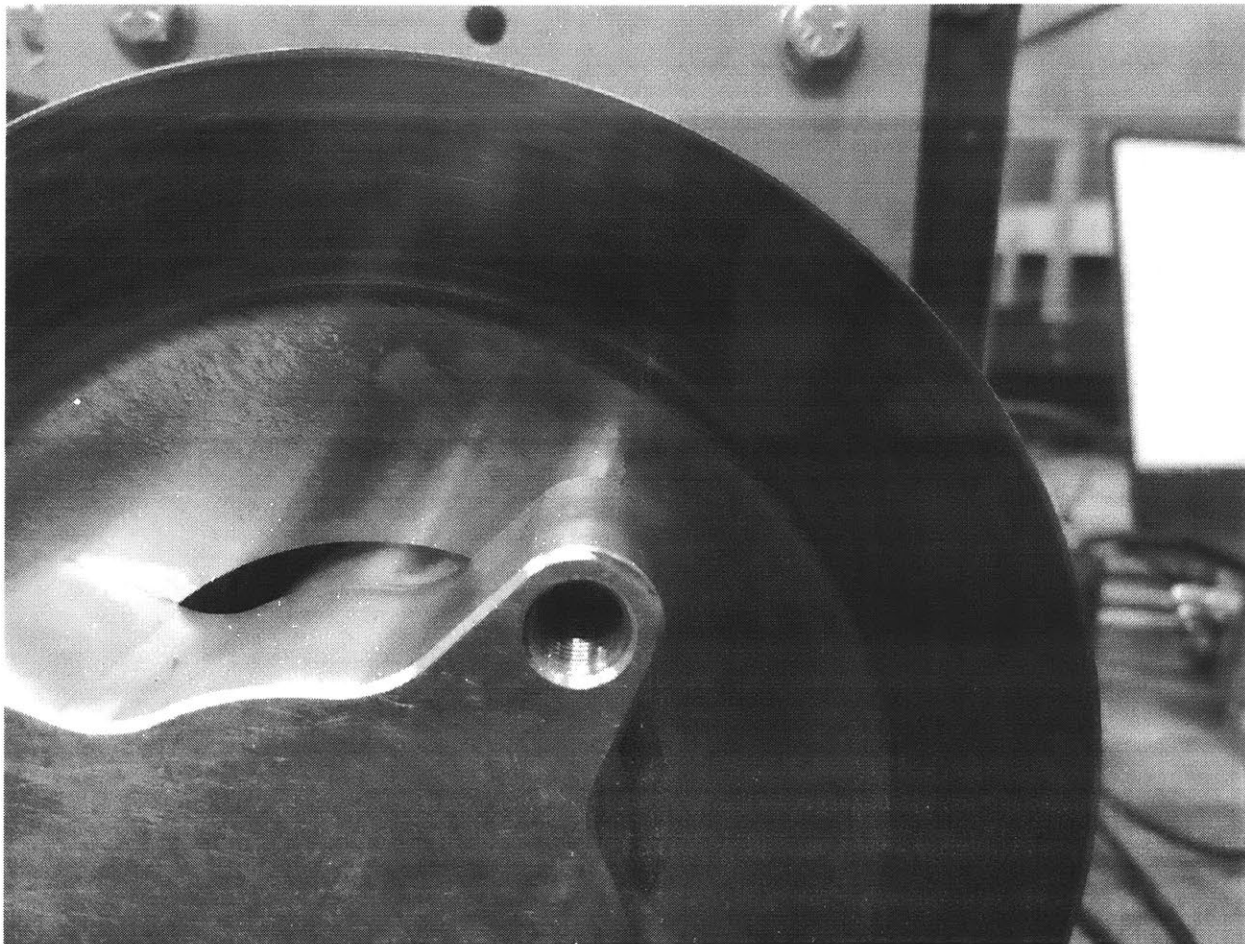
Figure 10. A photograph of the cast iron test rotor in post-test conditions. Note that a crack is propagating from the rotor's bolted joint with the aluminum hub. This rotor is made from Durabar G2 Cast Iron, which is a grey cast iron; this type of cast iron virtually lacks ductility and its ultimate strength is low compared to steel. Crack formation in the prototype rotor used for material selection did not inspire confidence in the material if it were to be selected for use in the braking system.

The 17-4PH stainless rotor also had some issues. It had the least consistent friction coefficient compared to the other two tested materials. This made 17-4 an unsuitable material for use on the MY18 braking system as well.

4130 steel alloy per AMS 6345 was chosen as the brake rotor material for the MY18 braking system. Even though it has the lowest average friction coefficient at 0.35, it still exceeds the minimum requirement of 0.32. 4130 alloy also has a weak dependence on temperature change and number of braking cycles which make it the ideal material for a braking system that is reliable and consistent.

3.4.2 ROTOR GEOMETRY CONCEPTS

A number of brake rotor geometry concepts were considered for use in the MY18 braking system. The rotor geometry has three main requirements:
1. The geometry must provide adequate cooling.
2. The geometry must minimize mass without compromising cooling effectiveness or the maximum braking torque.
3. The geometry must provide a means of allowing for the radial and axial thermal expansion of the rotor, without causing additional internal stresses in the rotor.

A floating rotor design was used to address the thermal expansion requirement. A typical floating rotor assembly consists of a brake carrier, the brake rotor, and brake rotor rivets or buttons. The carrier attaches to the wheel hub and provides an interface between the hub and the rotor. It is fixed with respect to the hub. The brake rotor is the part that interfaces with the brake pads. Braking torque from the brake rotor is transferred to the brake carrier with shear features and the brake rotor buttons. The brake rotor buttons act as pins for the shear features. The rotor-carrier interface is designed to allow for thermal expansion of the brake rotor while maintaining a torque transfer method via the shear feature.

The brake carrier and brake rotor buttons for the MY18 braking system use 17-4PH stainless steel for its excellent strength to weight ratio and it poor thermal conductivity. The high strength allows the brake carrier to be of lower mass compared to a lower strength steel. The poor thermal conductivity is desired to create a path of high thermal resistance between the extremely high temperatures of the brake rotor and the aluminum hub and precision bearings.

A number of brake rotor geometry concepts were considered for use on the braking system. Three concepts were chosen to be tested on the brake dynamometer to measure the geometry's total thermal resistance. This measurement could be used to select the brake rotor with the lowest thermal resistance and therefore the lowest steady state temperature.

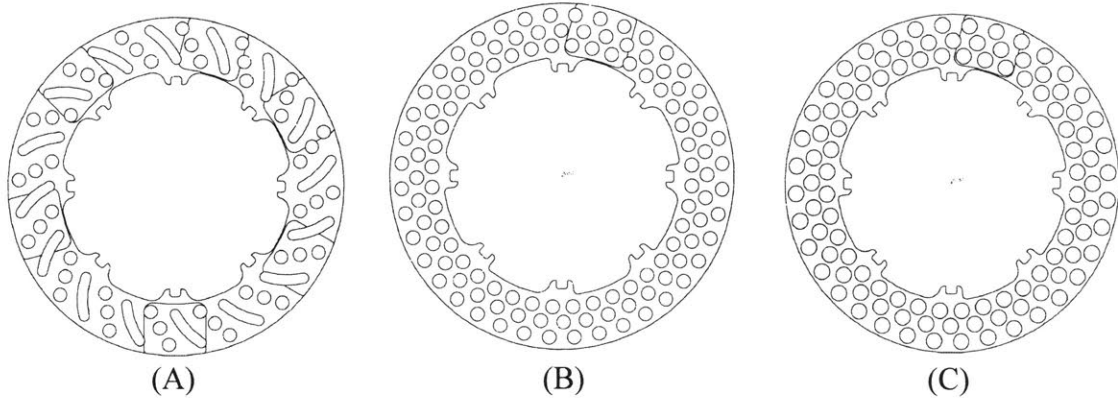The three rotors considered are depicted in figure 11.

25

Figure 11. Three conceptual rotors considered for cooling effectiveness testing. Rotor (A) is named "Holes and Slots" and features large slot cutouts that may help increase cooling. Rotor (B) is "Standard" and features hole cutouts with a radius equal to the thickness of the plate such that the net area change from the cutouts is zero. Rotor (C) is "Lite" and features large hole cutouts that significantly reduce the mass of the rotor. These concepts were chosen for their likelihood to produce good cooling performance as well as meeting the stress requirements of the braking load case.

3.4.3 ROTOR GEOMETRY FEM

Prior to being tested on the brake dynamometer, the geometry for each rotor concept was refined using a mechanical FEM simulation. The brake carrier and button geometry was also refined so that the entire assembly could be modeled together, increasing the accuracy of the results near the carrier-rotor interface.

The load case for the rotor assembly includes normal forces from the brake caliper and the braking torque acting on the surface intersection of the brake pad and the rotor. The maximum normal force and braking torque, which occurs at the front axle, was used for all rotors, such that front and rear rotor assemblies are interchangeable. Since the rotor has a patterned geometry, the resulting maximum stress will be a function of the angle where the loads are applied. Since the rotor has repeating geometry every 90°, loads were applied at 0, 15, 30, 45, 60, and 75 degrees. Once the angle with the highest stresses was identified, it was used as the primary load case.

Figures 12 and 13 show stress contour plots of the brake carrier. Material properties for this simulation were obtained from MMPDS-11. Please note that the yield strength of the material is 539 MPa at 500°C due to the yield strength of 17-4 being reduced at elevated temperatures. MMPDS-11 was also used for strength vs temperature data for the material. The yield strength on these plots is set as the color red in the plot's color bar.
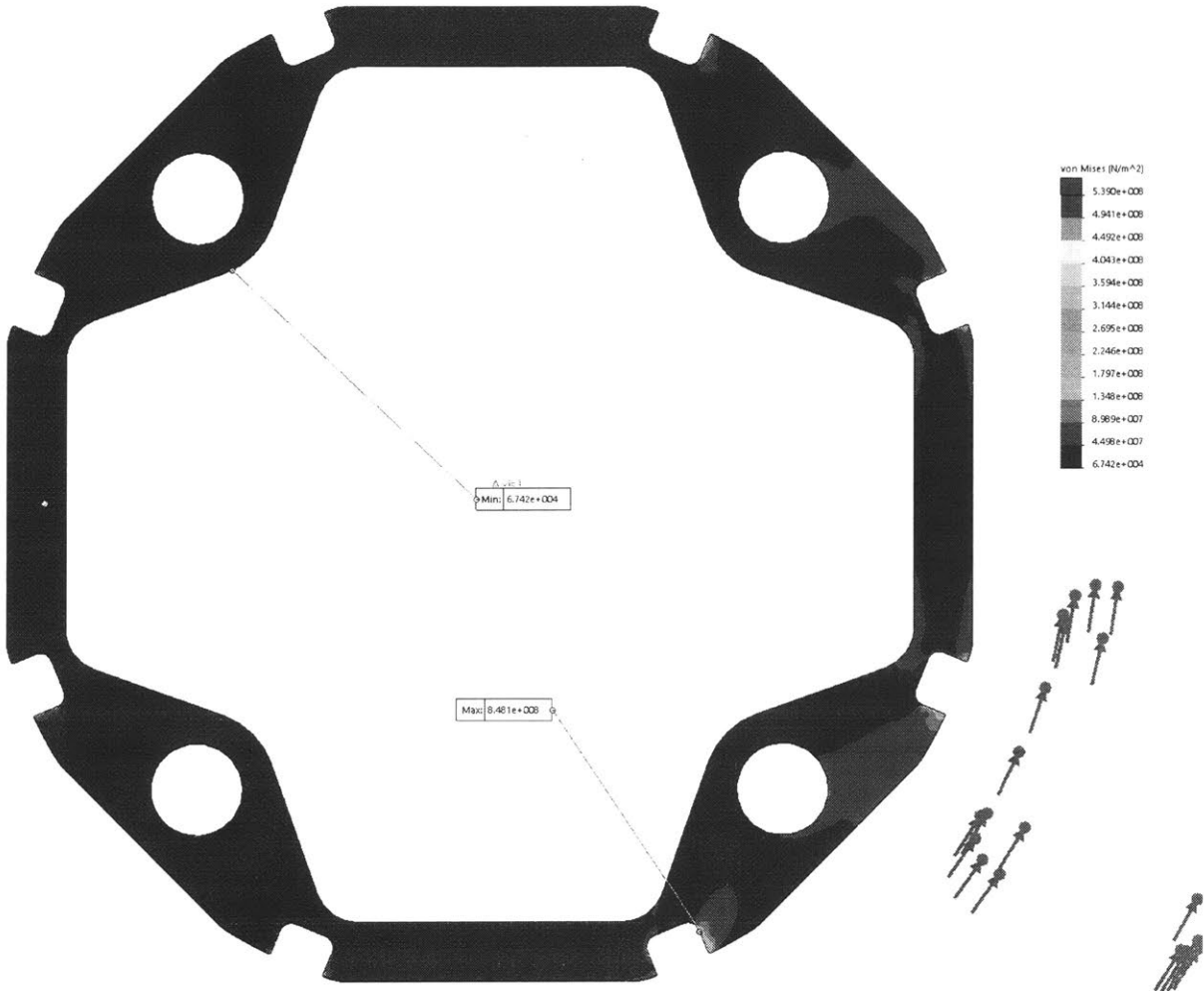
Figure 12. Stress contour plot of the brake carrier. This part fastens to the wheel hub and transmits torque from the brake rotor to the hub while allowing for radial and axial float of the rotor. The floating rotor mechanism is required to allow for thermal expansion of the brake rotor under elevated temperatures. 17-4 stainless steel is used for its extremly high strength as well as its poor thermal conductivity in the interest of thermally isolating the brake rotor temperature from the aluminum hubs and precision wheel bearings.
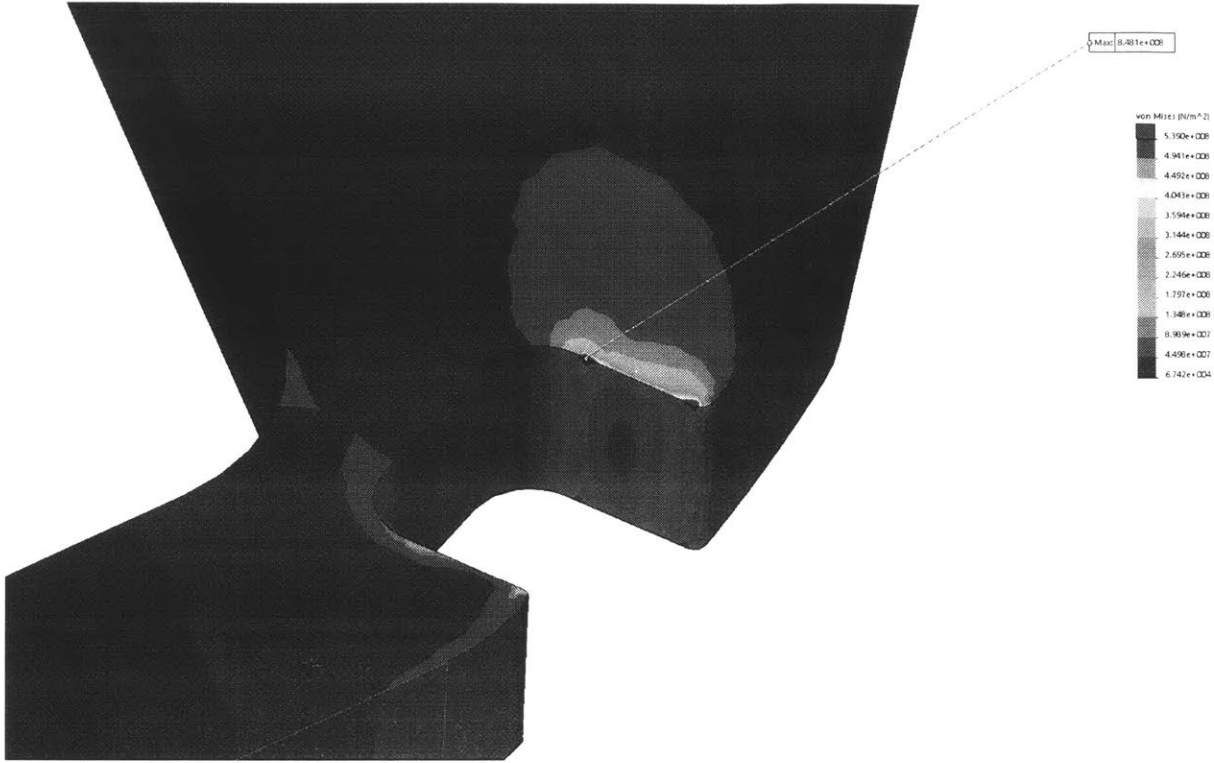
Figure 13. Stress contour plot of the 17-4PH stainless steel rotors, showing the shear feature in detail. Note that the peak stress is much higher than the allowable maximum stress. The peak stress is located at a boundry condition for this FE model, as well as a sharp corner in the geometry. The stress concentration was deemed acceptable since a majority of the material around the shear feature was significantly below the allowable stress limit.

The brake rotor stress contour plot for the "Lite" rotor concept is shown in figure 14. Recall that the rotors are made of 4130 steel alloy. The yield strength of the rotor is 279 MPa at 500°C. Once again this information was referenced from MMPDS-11. In the plot the color red corresponds to the yield strength of the material. The same analysis was used for the other two brake rotor concepts. The FEM was used to evaluate the stresses of the geometry and ensure that they were below the limit. Material was removed were possible in the interest of reducing weight. The final rotor geometry for the three concepts considered for dynamometer testing was completed and approved for manufacturing.
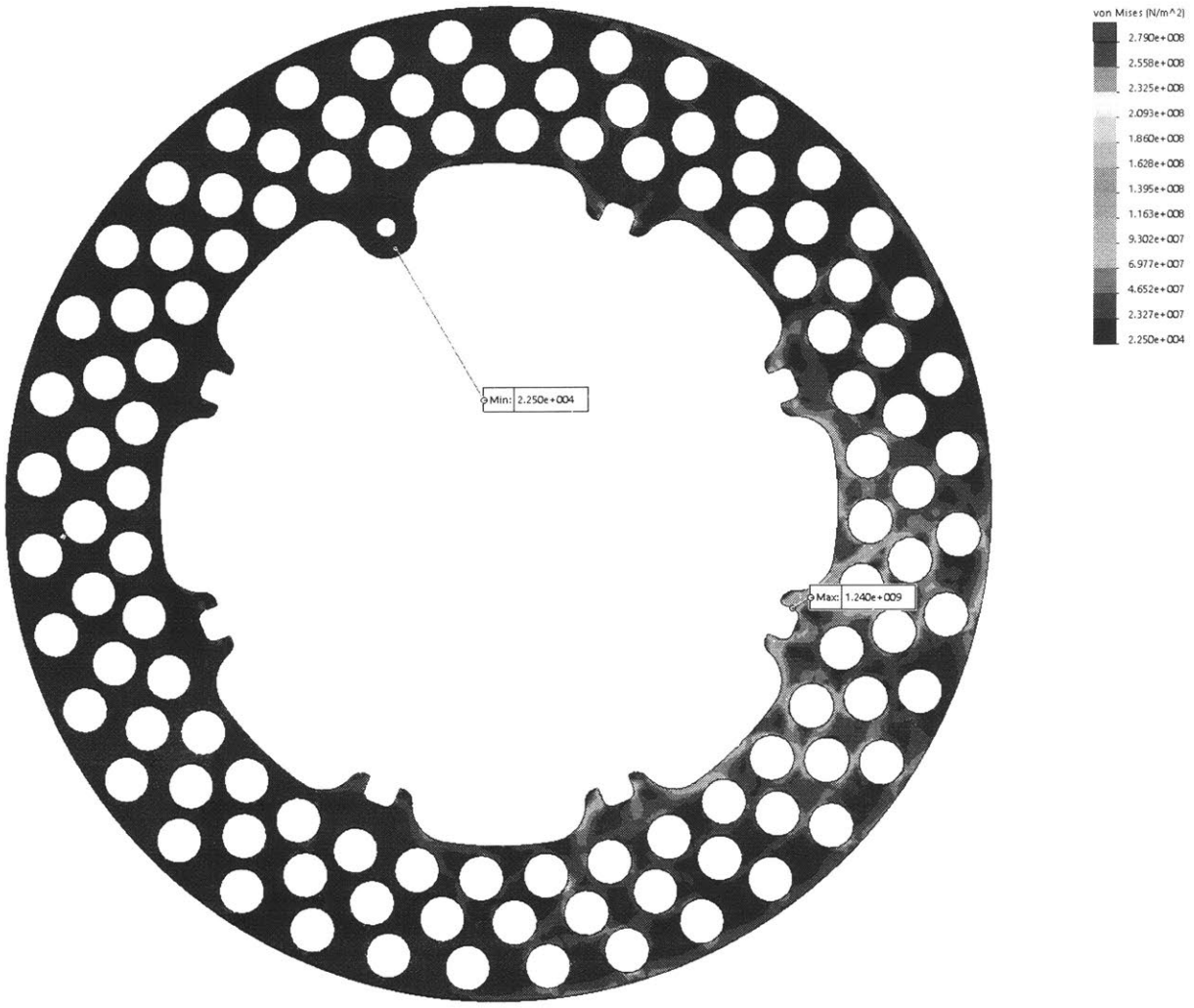
Figure 14. Stress contour plot for a conceptual brake rotor. The maximum allowable stress at 500°C was determined from MMPDS-11 data. This FE model was used to evaluate a number of brake rotor concepts to determine viable geometries given the load case the rotors must survive. Three concepts were selected for subsequent testing of cooling effectiveness.

3.4.4 ROTOR GEOMERTRY DYNAMOMETER TESTING

To determine the thermal resistance of the brake rotors, a lumped parameter model was assumed to described the bulk temperature of the brake rotors. The lumped parameter model fits well with thermal systems with a Biot number much smaller than one. Physically this means that the ratio of thermal conductivity and thermal convection results in very small thermal gradients in the mass being analyzed.

The lumped parameter model is summarized by equation (9).

$$\frac{dT}{dt} = \frac{-(T - T_{amb}) \cdot \frac{1}{R_{effective}} + \dot{Q}_{gen}}{m \cdot c} \qquad (9)$$

29

Solving this differential equation will yield the temperature vs time function given a set of initial and boundary conditions. One solution to this differential equation, given that $\dot{Q}_{gen} = 0$ is described by equation (10).

$$T = Ae^{-C \cdot t} + B \qquad (10)$$

The notable thing about this solution is that it is an exponential decay curve. The time constant of the decay carries significance as shown in equation (11).

$$R_{effective} = \frac{1}{C \cdot m \cdot c} \qquad (11)$$

Note that the effective thermal resistance can be calculated from the parameter C and the product of mass, m, and specific heat capacity, c of the material.

A test procedure to measure the thermal resistance on the brake dynamometer for the brake rotors is described as follows:
1. A brand new brake rotor and a set of brake pads is installed onto the brake dynamometer.
2. The FLIR thermal imaging camera is setup to record the brake rotor temperatures.
3. The pneumatic pressure is set to 40 PSI. The motor RPM is set to 1250 RPM, which represents the average speed of the vehicle on the endurance track.
4. The brake solenoid is opened such that a braking force is applied.
5. The solenoid is closed, and thus the braking force returns to zero when the maximum temperature of the brake rotor reaches 500°C
6. The rotor is allowed to cool back down to 100°C at a constant 1250 RPM. This is the cooling curve that will allow for the calculation of thermal resistance.
7. Steps 5 and 6 are repeated 3 times.

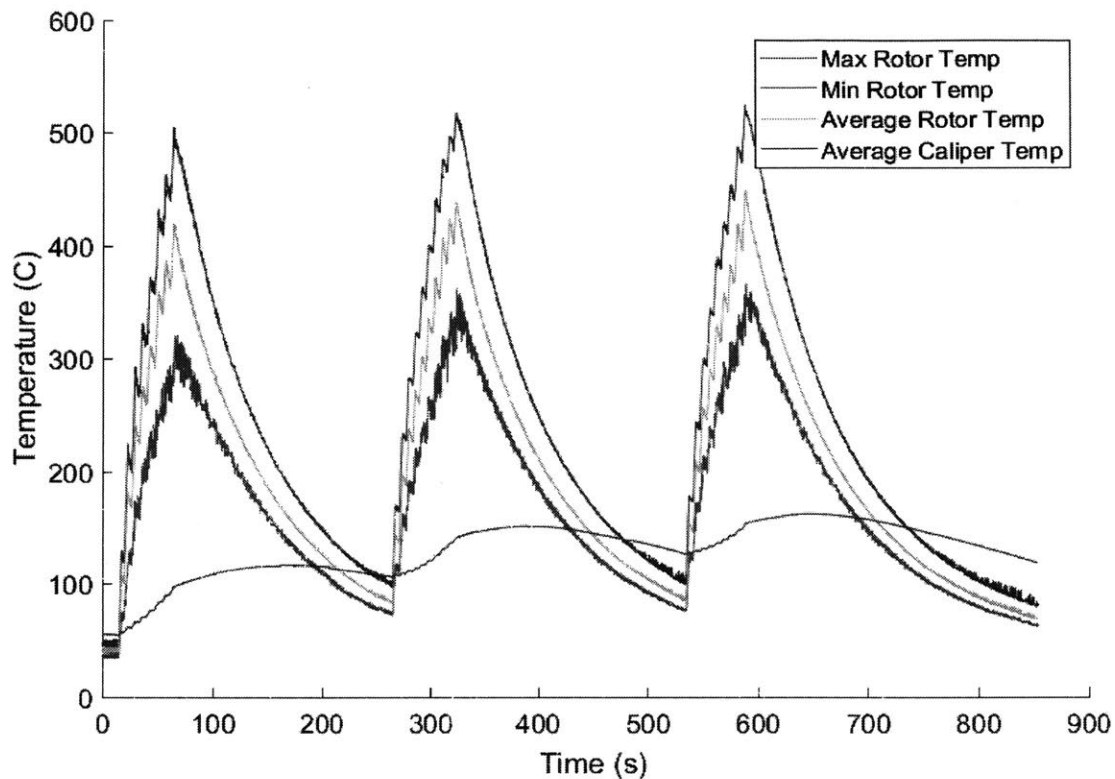Figure 15 shows raw data generated from the procedure described above.

Figure 15. Temperature vs time curves collected on the brake dyno used for calculating the effective thermal resistance of the rotors. Temperature was collected using a FLIR thermal imaging camera. A lumped parameter model was used to calculate the effective thermal resistance from the time constant of the cooling curve.

The FLIR thermal imaging camera logs temperature data from a sample window from the thermal image. Figure 16 shows a screenshot of a thermal image, where the white rectangle represents the sample window for temperature data logging. The minimum, average, and maximum temperatures within the sample window are recorded. For this particular image, the minimum temperature is not indicative of the minimum temperature on the surface of the rotor. This is because the rotor has cross drilled holes and the FLIR camera will report the temperature of objects behind the rotor.

The average and maximum rotor temperature data streams are more indicative of the rotor surface temperatures.
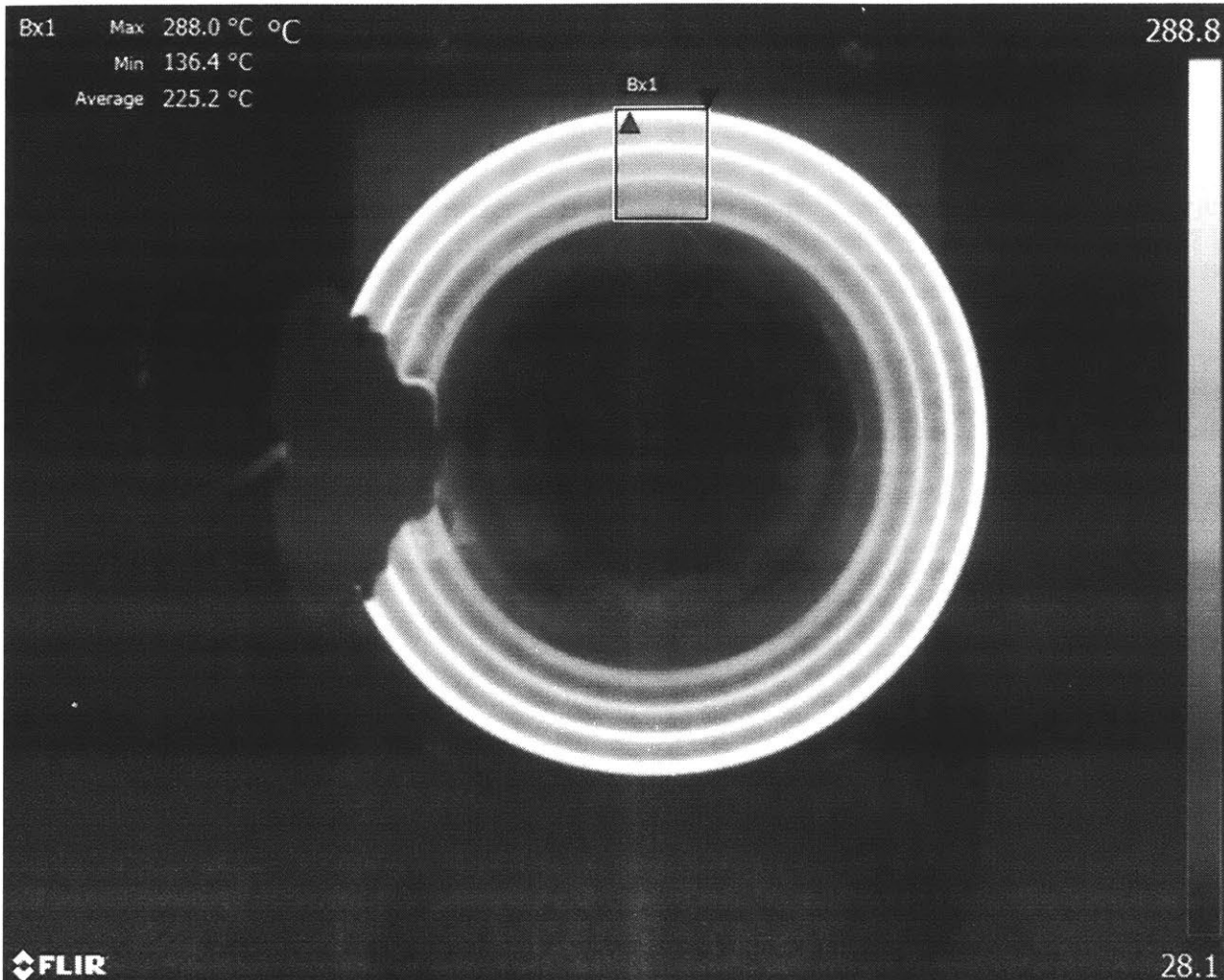
Figure 16. A thermal image captured during the cooling effectiveness tests. A bounding box was used to capture the maximum, average, and minimum temperatures of the brake rotor during the test. Because the brake rotor contains cutouts, some of the minimum temperature values may not be indicative of the actual minimum temperature on the brake rotor.

The average and maximum rotor temperature data streams are more indicative of the rotor surface temperatures. An exponential curve with the following general equation was fit to the cooling curves for the max and average temperatures for each of the three runs. Figures 17 and 18 show the exponential fit for one of the concept rotors. A thermal resistance for each of the cooling curves was calculated and then averaged across the three runs.
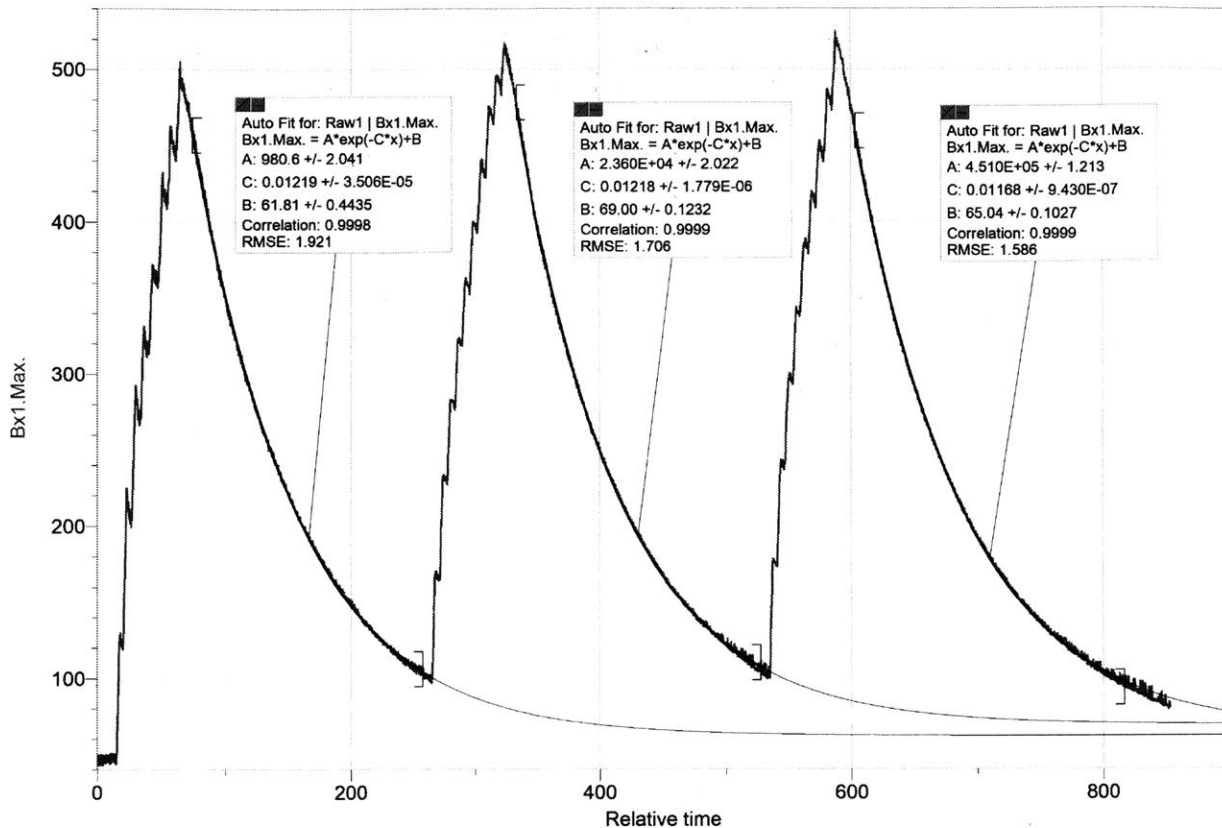
Figure 17. An exponential curve was fit to the cooling curve data for the maximum rotor temperature. The thermal time constant can be calculated from one of the coefficients from the exponential fit.
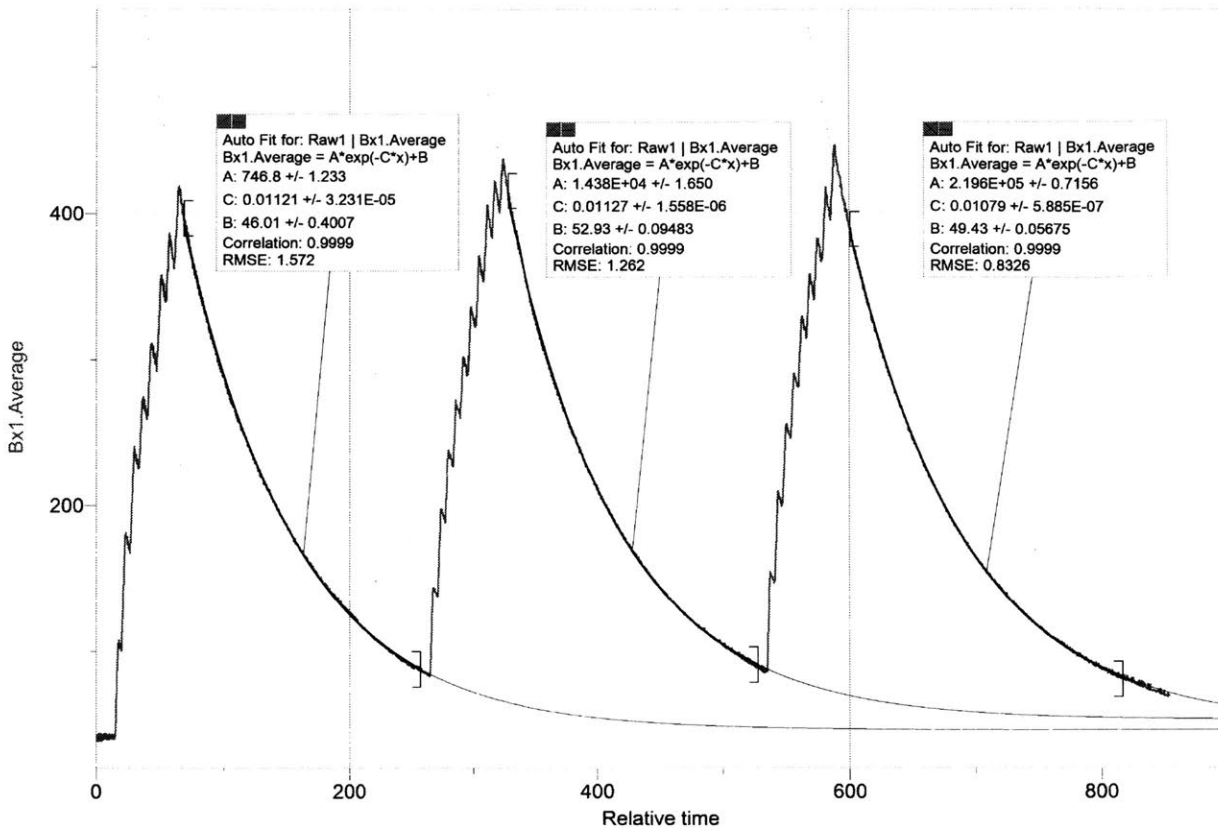
Figure 18. An exponential curve was fit to the cooling curve data for the average rotor temperature. The thermal time constant was compared to the time constant calculated for the maximum rotor temperature curve.

The "Lite" rotor had the lowest thermal resistance of the three different concepts. This rotor was also the most lightweight rotor. It was clear that this rotor was the best option for use in the MY18 vehicle. A comparison of the three different rotor concepts can be seen in figure 19 which is a temperature vs time plot of 5 laps of an endurance race. It shows how temperature fluctuates with the particular braking events around the circuit as well as show the steady state temperature of rotor given the measured thermal resistance.

This temperature vs time plot was generated by solving the lumped parameter model equation given that $\dot{Q}_{gen}$ is a function of time equal to the braking power. The braking power data is calculated from the LTS Study from Optimum Lap. The total breaking power is then divided among the 4 brakes on each wheel, and finally divided among power being dissipated via the brake rotor vs power being dissipated in the brake pad. 70% off braking power went to the front axle, 50% of that power goes to the front right brake, and 50% of that power is assumed to be dissipated by the brake rotor. Note that the steady state temperatures predicted by the model are above 500°C. This model is used for comparative purposes among the different brake rotor concepts. The model is a simplification of the thermal system and may not accurately predict reality.
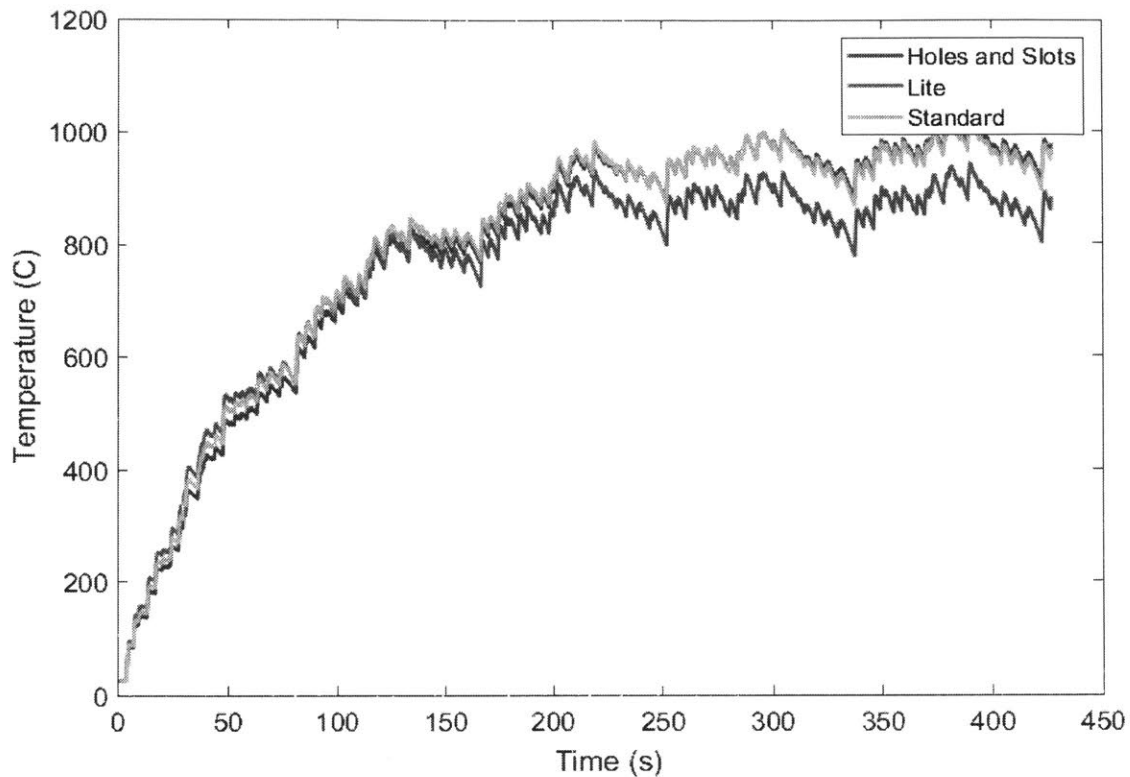
34

Figure 19. Simulation of brake rotor temperature vs time throughout 5 laps. Braking power data was calculated from the output of a laptime simulation, and fed into a lumped parameter thermal model of the brake rotors. This simulation was used to compare the thermal performance of each of the different rotor concepts using the measured thermal resistance in the lumped parameter model. The thermal performance between "Lite" and "Standard" is very similar; "Holes and Slots" has a significantly higher thermal resistance and reaches a higher steady state temperature.

The model affirms that the "Lite" rotor will result in a lower steady state temperature compared to the other rotor concepts. The model also reveals that the "Lite" rotor, with its reduced mass, will get to the steady state temperature in a shorter amount of time.
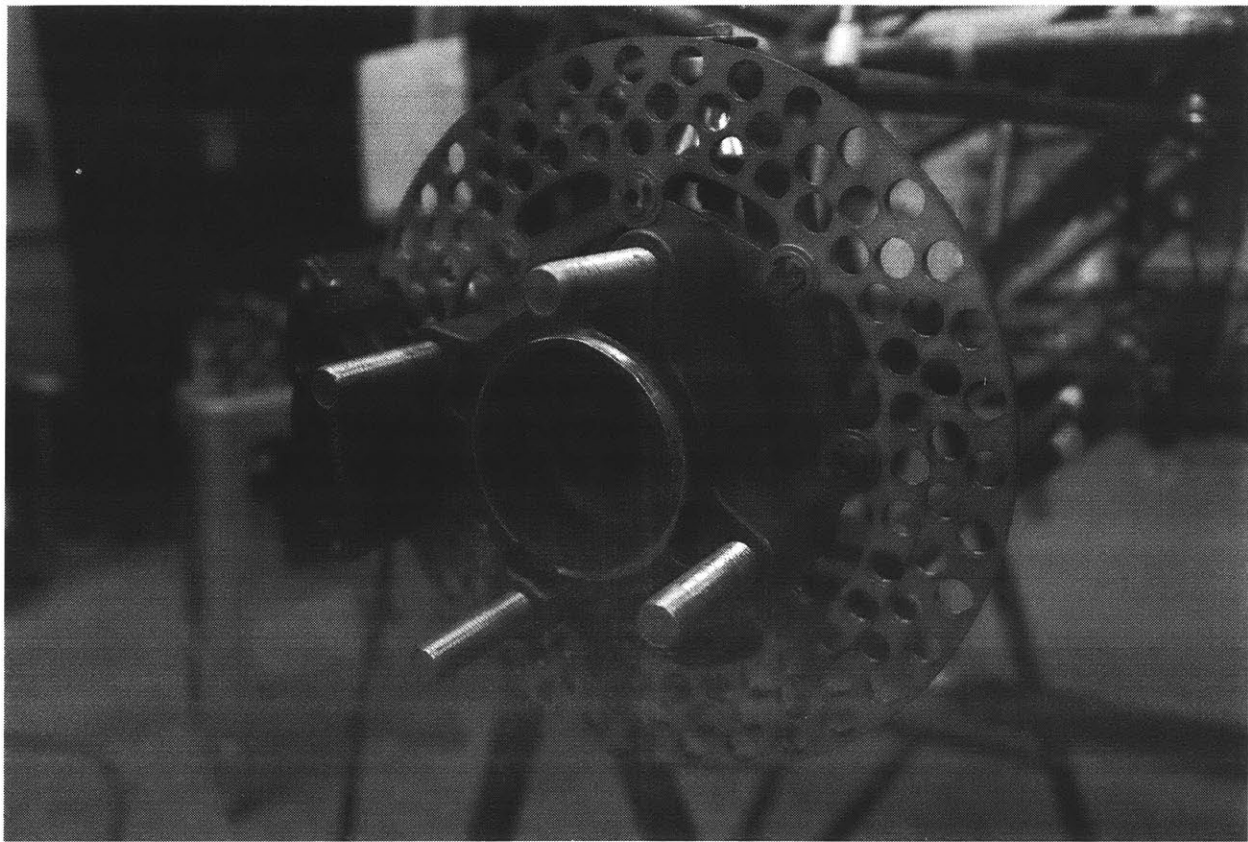
Figure 20. An integrated brake rotor assembly on the front wheel package assembly.

3.5 REGENERATIVE BRAKING

The regenerative braking system aims to recover energy from braking events to be restored to the battery pack. According to the power vs time output of the LTS study, more than 1 kW-Hr of energy can be recovered from the rear brakes alone. MY18 electric rear wheel drive architecture allows for a simple method for controlling the amount of braking torque output by the regenerative braking system.

The electric powertrain is controlled by means of a torque command. Positive torque commands result in forward motion of the vehicle. Negative torque commands while the motor is still spinning in the forward direction will not only create a braking torque, but will result in negative power into the battery, thus energy is recovered. The car's VCU must be able to determine what the appropriate amount of torque to send to the motor controller is given the driver inputs to the accelerator and brake pedals.

The brake lines have pressure transducers such that the VCU can make calculations based on the brake pressure values. The VCU will need to make the following calculations:

$$\tau_{CMD,motor,regen} = k_1 \cdot P_f \cdot \left(\frac{1}{BB_{e,f}} - 1 \right) \tag{12}$$

Where,

$$k_1 = \frac{\mu_{pad-rotor} \cdot 2 \cdot r_{rotor,effective} \cdot A_{C,f}}{GR} \tag{13}$$

P_f is the measured hydraulic pressure in the front brake lines. $BB_{e,f}$ is a user defined variable that represents the electronic brake balance distribution. This value can be changed by the driver to satisfy their driving preferences. All other variables are constants that describe the physical system. For example, GR is the gear ratio in the powertrain. Note that the braking torque command is directly proportional to the front braking pressure, hence giving the driver direct control over the braking torque.

The VCU will also have to decide if the appropriate conditions are met to allow a negative torque command to be sent to the powertrain. The any of the following conditions will override the regen torque command from the above calculation and set the torque command to zero:
- If the vehicle speed is below 5 kph
- If the accelerator pedal is pushed more than 5%
- If the brake shutoff valve is not in the closed condition
- If the rear brake pressure exceeds a threshold
- If the front brake pressure is below a threshold
- If the battery bus voltage is greater than 300V

The driver must "activate" the regenerative braking feature via an interactive menu on the dashboard. When the feature is activated, the brake shutoff valve is put in the closed position. The following conditions will cause the brake shutoff valve to be in the open position:
- If LV power is shutoff
- If an E-stop button is pressed
- If the motor controller is disabled
- If the rear brake pressure exceeds a threshold
- If it is detected that a brake pressure sensor has failed

These conditions are intended for the protection and safety of the driver or nearby people. The regenerative braking system can be very dangerous since it controls the torque output of the motor.

3.5.1 REGENERATIVE BRAKING PSUEDO-CODE

```
%%%%%%%%%%%%%%%%%%%%%%%%%%%%%%%%%%%%%%%%%%
%          Variables
%%%%%%%%%%%%%%%%%%%%%%%%%%%%%%%%%%%%%%%%%%

regen_torque_CMD
speed_car
speed_motor
battery_voltage
accelerator
brake_pressure_front
brake_pressure_rear
k
BB_e_f % <------ This variable needs to be able to be adjusted from the dashboard.


%%%%%%%%%%%%%%%%%%%%%%%%%%%%%%%%%%%%%%%%%%
%          Thresholds
%%%%%%%%%%%%%%%%%%%%%%%%%%%%%%%%%%%%%%%%%%

speed_car_threshold = 5 kph;
speed_motor_threshold = 250 RPM;
brake_pressure_rear_threshold = 120 PSI;
brake_pressure_front_threshold = 120 PSI;
battery_voltage_maximum_threshold = 299 V;
accelerator_maximum_threshold = 5%;
regen_torque_CMD_maximum = 100 Nm;


%%%%%%%%%%%%%%%%%%%%%%%%%%%%%%%%%%%%%%%%%%
%          State Variables
%%%%%%%%%%%%%%%%%%%%%%%%%%%%%%%%%%%%%%%%%%

% 1 = on/pressed; 0 = off/released;

motor_controller_enable_state
brake_shutoff_valve_state
regen_feature_state
HV_state


%%%%%%%%%%%%%%%%%%%%%%%%%%%%%%%%%%%%%%%%%%
%          Regen Controller
%%%%%%%%%%%%%%%%%%%%%%%%%%%%%%%%%%%%%%%%%%

if HV_state == 1
        AND regen_feature_state == 1
        AND motor_controller_enable_state == 1
        AND brake_pressure_rear < brake_pressure_rear_threshold
then
        brake_shutoff_valve_state == 1;
else
        brake_shutoff_valve_state == 0;
end
```

```
if brake_shutoff_valve_state == 1
        AND speed_car > speed_car_threshold
        AND speed_motor > speed_motor_threshold
        AND accelerator < accelerator_maximum_threshold
        AND battery_voltage < battery_voltage_maximum_threshold
        AND brake_pressure_front > brake_pressure_front_threshold
then
        regen_torque_CMD = k*brake_pressure_front*((1/BB_e_f)-1);

        if regen_torque_CMD > regen_torque_CMD_maximum
        then regen_torque_CMD = regen_torque_CMD_maximum;

else
        regen_torque_CMD = 0;
```

4. FUTURE WORK

While the design work for the MY18 was quite extensive, a number of recommendations are made in this section for future work that may increase the performance of future braking systems.

With regards to brake pads, it is recommended that custom brake pads be commissioned for further brake dynamometer testing. A manufacturer named Porterfield Racing Brake Pads has the ability of manufacturing brake pads compatible with the Wilwood GP200 brake calipers. These brake pads should be compared to the brake pads currently being used, in case significant gains in coefficient of friction can be made. An increase in the coefficient will decrease the system's hydraulic pressure. These new brake pads should be tested with 17-4PH stainless steel again in the case that better consistency can be achieved. The same procedure defined in this document can be used such that results for the new brake pads can be compared to the results for the stock Wilwood brake pads.

Regarding the thermal resistance measurement, it is recommended that the thermal resistance as a function of wheel RPM be measured. The new data could then be used to generate a more accurate lumped parameter model with variable thermal resistance to predict the brake rotor temperatures.

With regards to the amount of power actually being dissipated by the brake rotor, it is recommended that a test on the brake dynamometer be conducted to find out how much power is dissipated in the brake rotors vs the brake pads. If the mechanical power into the brake dyno is measured, and if the brake rotor temperature is measured then the distribution of power going to the brake rotors can be calculated.

It is also recommended that the brake pad temperatures during a race or a testing session be logged for the purposes of validating the cooling design and making sure that pad temperatures stay below the design limit.

For the regenerative brake system, it is recommended that acceleration measurements be incorporated in the electronic brake bias setting. The brake bias can be dynamically adjusted based on the vehicles actual state of acceleration. Recall that as deceleration increases more and more load gets transferred to the front axle.

5. REFERENCES

1. Milliken, Douglas L., and William F. Milliken. Race Car Vehicle Dynamics. Warrendale: Society of Automotive Engineers (SAE), 1995. Print.
2. Pacejka, H.B. (2012) Tire and Vehicle Dynamics. 3rd Edition, Butterworth-Heinemann, Oxford.
3. Smith, Carrol, Prepare To Win, Aero Publishers Inc., Fallbrook CA, 1975.